Available online at www.sciencedirect.com
SCIENCE DIRECT®
Precambrian Research 143 (2005) 50–74
Precambrian Research
www.elsevier.com/locate/precamres

Structural complexity in the Curnamona Province (South Australia): Polyphase strain partitioning and reactivation

Jérôme Ganne *, P.G. Betts, R. Weinberg, M. Noble

Australian Crustal Research Centre, School of Geosciences, Monash University, P.O. Box 28E, Melbourne, Vic. 3800, Australia

Received 9 September 2004; received in revised form 26 August 2005; accepted 20 September 2005

Abstract

In this paper, we examine the apparent timing relationships between the structural and metamorphic events of the amphibolite facies sequence in the Walter-Outalpa Shear Zone (WOSZ) area in the southwestern part of the Palaeo- to Mesoproterozoic Curnamona Province. The local structural geometry and style are largely due to heterogeneous, non-coaxial flow in which foliation development is related to the superposition of two main independent structural events (D2* and D3*). Strain was progressively partitioned into high-strain zones in the southern part of the study area in contrast to the low-strain areas in the north of the study area. D2* deformation developed under amphibolite facies conditions and is partitioned between zones of thrusting and flattening (±folding) related to nappe formation. D3* deformation developed under greenschist facies conditions and is partitioned between strike-slip faulting and folding. D3* high-strain zones form discontinuous, NW-trending anastomosing strands that contain relics of the D2* thrust-related foliation. These relicts preserve the higher grade mineral assemblages that are partially overprinted by D3* retrograde assemblages. Strike-slip movement along the WOSZ is, therefore, interpreted to have re-used the pre-existing D2* thrust such that D2*-strain partitioning influenced renewed D3* strain partitioning.

The high-grade metamorphism and phase of pervasive deformation (D2*/M2) are ascribed to the D2 Mesoproterozoic Olarian Orogeny that occurred in the Curnamona Province between ca. 1600 and 1590 Ma. The tectonic context of the D3*/M3 shearing event is highly uncertain. Recent geochronological Sm–Nd isotope ages from garnet from within the WOSZ shear zone yield ca. 520–490 Ma Delamerian ages [Dutch, R.A., Hand, M., Clark, C., 2005. Cambrian reworking of the southern Australian Proterozoic Curnamona Province; constraints from regional shear zone systems. Geol. Soc. London 162; 5, 763–775]. However, the D3*M3 shear foliation are truncated by the Neoproterozoic unconformity flooring the Adelaide Rift Complex stratigraphy, suggesting pre-Delamerian Orogeny activity along the shear zone. It is, thus, likely that the D3* movement along the shear zone records a combination of late Olarian Orogenic movement with a component of reactivation during the Delamerian Orogeny.

Keywords: Shear zones; Strain partitioning; Reactivation; Proterozoic; High-grade metamorphism

1. Introduction

1.1. High-strain zones

High-strain zones are common in a variety of tectonic settings and structural geologists have long sought to understand their kinematic significance. Understanding the kinematic significance of high-strain zones requires knowledge of their finite deformation symmetry,

* Corresponding author. Tel.: +61 3 9905 3097.
E-mail address: jganne@univ-fcomte.fr (J. Ganne).

0301-9268/$ – see front matter © 2005 Elsevier B.V. All rights reserved.
doi:10.1016/j.precamres.2005.09.010

rotational strain (vorticity), three-dimensional strain and volume change. Such kinematic information should subsequently be combined with an interpretation of the tectonic transport direction and the mode of deformation (strike-parallel, oblique, or dip-parallel transport) to fully understand the overall tectonic significance of the high-strain zones. Such kinematic analysis often relies on determining the geometry of foliations and lineations within high-strain zones to establish their kinematic significance, and therefore, to construct tectonic histories. As discussed by Reddy and Occhipinti (2004), the basis for this streamlined approach has been the assumption that shear zones deform by simple shear: a situation that allows mineral lineations within the zone to be related to transport directions (Ramsay, 1980; Hanmer & Passchier, 1991, Goodge et al., 1993; Wheeler & Butler, 1993; Passchier, 1994) (Ramsay, 1980; Hanmer and Passchier, 1991; Goodge et al., 1993; Wheeler and Butler, 1993; Passchier, 1994). During natural deformation, simple shear is unlikely to be the only deformational process operating. Instead, a combination of pure and simple shear (general shear) is likely to occur (Bailey and Eyster, 2003).

Detailed field studies and recent theoretical modelling of high-strain zones have recognised complexities that cannot be ascribed to a single, simple-shear deformation (Sanderson and Marchini, 1984; Fossen and Tikoff, 1993; Robin and Cruden, 1994; Tikoff and Teyssier, 1994; Jones et al., 1997; Fossen and Tikoff, 1998; Jiang and Williams, 1998; Lin et al., 1998; Passchier, 1998; Jiang and Williams, 1999; Reddy and Occhipinti, 2004). The deformation in such zones is commonly interpreted in terms of a polyphase deformation history because high-strain zones are rheologically weak and may undergo reactivation during subsequent deformation (Butler et al., 1997). Reactivation criteria (Holdsworth et al., 1997) must then be identified to support such an interpretation. However, evidence for reactivation may be absent or equivocal and alternative interpretations involving ‘general shear’ may be more valid. Consequently, establishing the structural evolution of high-strain zones is a complex and difficult subject. However, recognising the differences between ‘general shear’ and polyphase deformation is crucial for correctly interpreting the tectonic context of the shear zone. Failure to do so will lead to misinterpretations of tectonic history. Thus, there is still a need to make observations from within high-strain zones, and to assemble them in current conceptual frameworks.

In this paper, a detailed field and microstructural petrological study of a kilometric-scale shear zone, the Walter-Outalpa Shear Zone (WOSZ), is used to demonstrate (a) that the processes of deformation partitioning have been important in the production of structural geometries developed at all scales; (b) that early formed fabrics resulting from strain partitioning controlled subsequent strain partitioning; and (c) that detailed microstructural and metamorphic analysis provides new evidence that links the different steps in the evolution of the WOSZ with that of regional folds.

Such studies are important in Precambrian terranes, such as the Curnamona Province, where poly-orogenic and metamorphic evolutions result in complicated three-dimensional geometries, overprinting relationships and complex and episodic movement histories along shear zones. As such, the context of structural features such as shear zones are often misinterpreted and their tectonic significance misconstrued.

1.2. Structural complexity in the Curnamona Province

Our investigation was undertaken in the southern Curnamona Province, South Australia (Fig. 1). This province preserves evidence for multiple tectonic events of varying intensities of deformation and metamorphism (Vernon, 1969; Berry et al., 1978; Archibald, 1980; Hobbs et al., 1984; Clarke et al., 1986; Stevens et al., 1988; Cook and Ashley, 1992; Flint and Parker, 1993; Robertson et al., 1998; Flint, 2002; Gibson and Nutman, 2004). Despite extensive documentation of stratigraphic (Stevens et al., 1988; Conor, 2004; Fig. 2), structural and geochronological constraints on the evolution of the Curnamona Province (for a review see Raetz et al., 2002), there are still considerable ambiguities regarding the tectonic regime and processes responsible for the regional deformation and metamorphism (Tables 1 and 2). There is a general consensus that deformation and metamorphism occurred during two orogenic cycles. The first orogenic cycle was identified as the Palaeo- to Mesoproterozoic Olarian Orogeny (ca. 1600–1590 Ma; Page et al., 2000). It is characterised by intense poly-deformation and high-temperature metamorphism interpreted to be the result of Proterozoic collision between Australia and Laurentia (Betts et al., 2002). The second orogenic cycle termed the Delamerian Orogeny occurred during the Cambrian (ca. 520–490 Ma; Harrison and McDougall, 1981). Evidence for the Delamerian Orogeny is preserved within the Paleoproterozoic (1720–1640 Ma) Willyama Supergroup (Stevens et al., 1988; Conor, 2004) and the unconformably overlying Neoproterozoic (830–700 Ma) Adelaide Rift Complex (Preiss, 2000). The Delamerian Orogeny is interpreted to be related to accretion

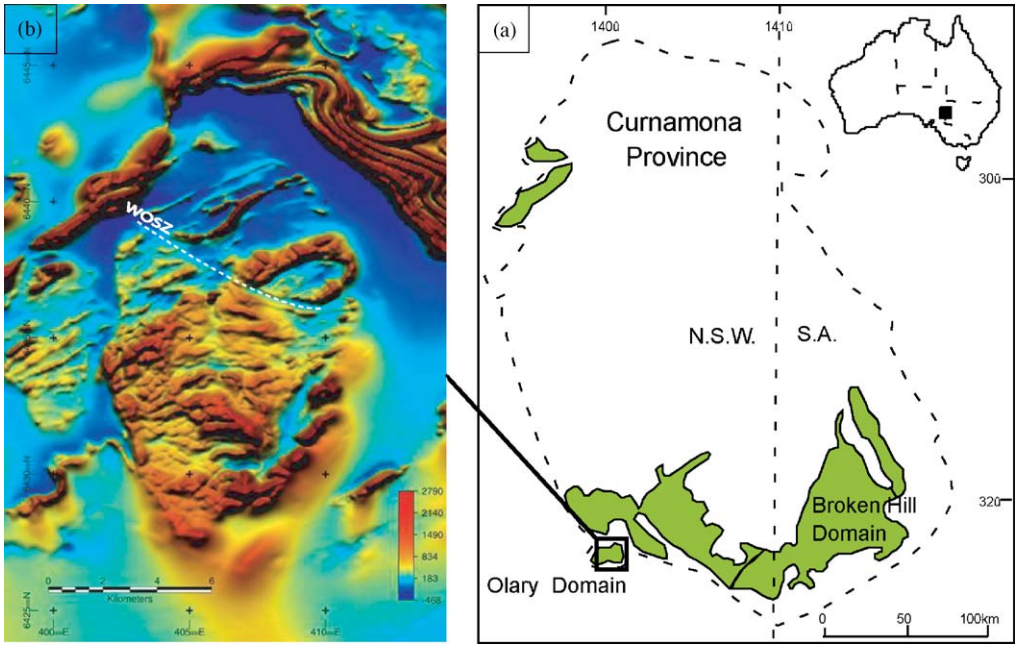

Fig. 1. (a) Simplified map of the Curnamona Province showing geographically defined Olary and Broken Hill Domains. (b) Magnetic image of the Weekeroo Inlier showing the kilometric-scale Walter-Outalpa Shear Zone (WOSZ). This contact defined with shared redox boundary (Gibson and Nutman, 2004) separating the Curnamona (migmatic bodies in the south) and Strathearn Groups (pelitic sequence in the north, see Fig. 3).

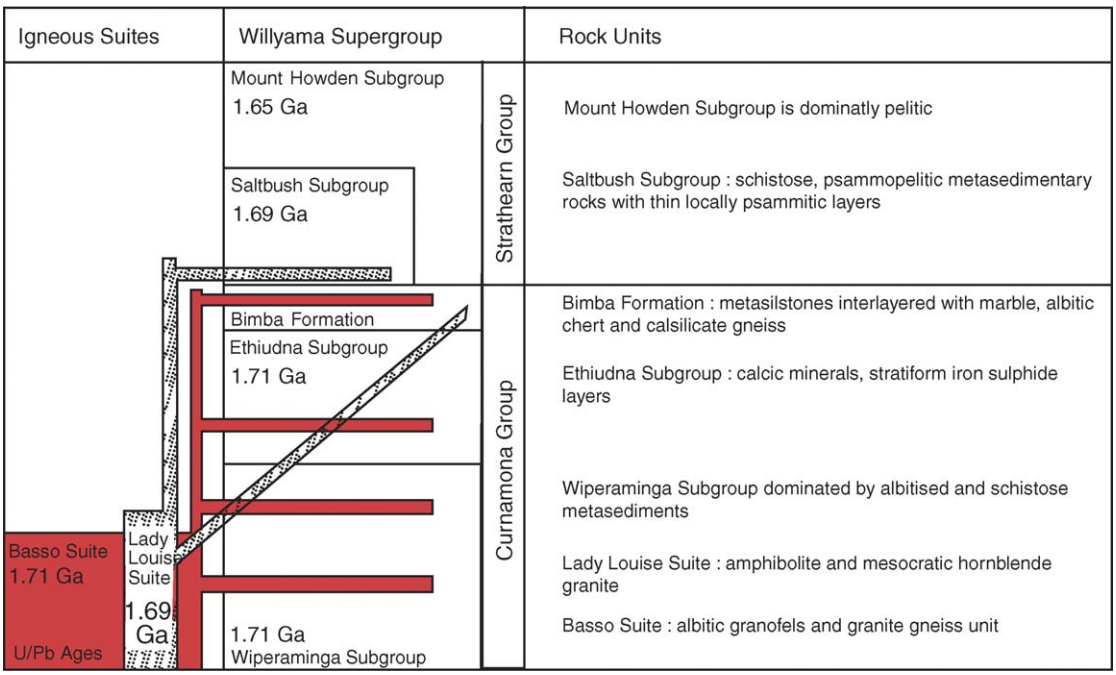

Fig. 2. Major stratigraphic units in the Olary Domain (after Conor, 2000; modified).

Table 1
Alternative structural histories and nomenclatures adopted by various investigators for different deformational/folding events in Olary Domain

Berry et al. (1978)	Archibald (1980)	Clarke et al. (1986)	Flint and Parker (1993); Flint (2002)	Gibson (2002)	This study
Olarian Orogeny					
D1 (layer-parallel fabric; folds isoclinal and recumbent)	D1 (layer-parallel fabric; folds isoclinal and recumbent)	D1 (SE-directed nappe structures with shallow-dipping axial plan fabric)	D1 (layer-parallel fabric; folds isoclinal and recumbent)	D1 (layer-parallel fabric; no folds recognised)	D1* (layer-parallel fabric; no folds recognised)
D2 (weak)	D2 (weak)	NR	D2 (tight to isoclinal upright NE-trending folds with steeply dipping axial plane fabric)	D2 (non-cylindrical, tight to isoclinal, reclined to recumbent folds; NW–SE trend dominant)	D2* (reclined recumbent folds; NW–SE trending thrusts)
D3 (upright)	D3 (upright) RSZ	D2 (upright) D3 (+RSZ)	D3 (upright) RSZ	D3 (upright folds D4 (+RSZ)	D3* (upright folds trending NW–SE; transpressional fault)
Delamarian Orogeny				Not investigated	
D4	Not investigated	Not investigated	D4		Not investigated
D5			D5		

RSZ = retrograde shear zone; NR = not recognised.

strain partitioning

along the eastern margin of Gondwana (Betts et al., 2002).

Studies by Hobbs et al. (1984), Gibson (2000), Wilson and Powell (2001), Forbes et al. (2004) and Forbes and Betts (2004) in the Curnamona Province indicate that major shear zones active during amphibolite to greenschist facies metamorphism have complicated foliation and lineation distributions. Many workers (e.g. Rutland and Etherridge, 1975; Glen et al., 1977; Berry et al., 1978; Laing et al., 1978; Corbett and Phillips, 1981; Clarke et al., 1986; Flint and Parker, 1993) have assumed that the amphibolite- and greenschist-grade shear zones formed during the retrograde evolution of the Olarian Orogeny. This assumption is, in part, based on structural arguments and limited thermochronological data. An important consequence of linking the shear zone mineral assemblage to the waning stages of Olarian Orogeny is that they inevitably leads to the conclusion that metamorphism during orogenesis followed an anticlockwise *P–T* path and isobaric cooling history (Clarke et al., 1986, 1995). These shear zones have been mapped at a regional-scale and their structural and kinematic evolution has been interpreted in several ways (see Table 1). For example, early high-temperature shear zones have been attributed in recent studies to D1 extensional tectonics (Gibson and Nutman, 2004), thrusts that sole regional nappes (White et al., 1995; Forbes et al., 2004; Forbes and Betts, 2004) and as zone of transpression (Wilson and Powell, 2001). Documenting and undertaking this complex evolution is a necessary step to accurately describe the structural evolution of the Curnamona Province.

Our tectonic investigation falls within the frame of an active interest for strain localization and high-grade metamorphism in the Curnamona Province (Dutch et al., 2005). The spirit of this paper was driven in the light of stimulating models proposed by Hobbs et al. (1984) and more recently Wilson and Powell (2001) that challenged the interpretation of high-strain zones in the Curnamona Province and reinterpreted the Broken Hill Block as a series of discrete early high-grade structure packages, separated from their neighbours by late high-angle strike-slip faults.

2. Definition of strain-related terms used in this paper

2.1. Deformation partitioning

This term is used as defined by Bell (1981), where partitioning of strain in a progressively deforming rock mass is viewed as a tectonic process, which accommo-

Table 2
Mineral assemblages and fabrics associated with D1–D3 deformational events for the Strathearn Group (after Gibson and Nutman, 2004)

Event	Strathearn Groups
D1–M1	Andalusite, muscovite, biotite, quartz, garnet, plagioclase, fluorite, tourmaline in metapelitic rocks; K-feldspar and fibrolite in higher grade metapelitic rocks; layer-parallel S1 fabric
D2–M2	Andalusite locally stable in metapelitic rocks at higher structural levels; fibrolite, sillimanite, biotite, garnet, K-feldspar, quartz, plagioclase at deeper levels sub-horizontal to gently dipping S2 fabric; limited partial melting along S2 surface
D3–M3	Staurolite, biotite, muscovite, quartz, garnet, chloritoid in pelitic rocks; steeply dipping S3 foliation

Mineral assemblages listed in the table define the M1, M2 and M3 peak of metamorphism.

dates progressive shearing strain. Strain can be further subdivided into regions undergoing: (1) no strain; (2) dominantly progressive shortening plus shearing strain; (3) progressive shortening plus shearing strain; and (4) progressive shearing-only strain.

2.2. Regional strain

This term is used as defined by Means (1994), and then Bell et al. (1986). When strain is partitioned, the regional or bulk strain is the sum of the partial strains (terminology after Means, 1994) contributed by domains at a lesser scale. In this case, the term *regional* or *bulk* refers to the scale of the Olary Domain described herein. The bulk strain can be further considered in terms of bulk shear strain and bulk shortening strain. In this paper, the *bulk shear sense* relates to the sense of shear operating at the scale necessary to form the tectonic features of the WOSZ area.

2.3. Re-use or reactivation

This term is used as defined by Bell et al. (1986), then Davis and Forde (1994), and refers to the accommodation of progressive strain by pre-existing foliations during a subsequent deformation.

2.4. Reworking

This term is used as defined by Reddy et al. (2003). It requires that high-strain structures developed in the early stages of the deformation are subsequently overprinted by younger stages of the same deformation.

3. Geological setting of the Curnamona Province

The Curnamona Province stands out prominently as is a sub-circular magnetic anomaly on the aeromagnetic map of Australia. Palaeoproterozoic outcrops are restricted to the Olary and Broken Hill domains in the southern part of the province and to small inliers (Mount Painter and Mount Babbage) in the northwest (Fig. 1). The remainder of the province is shallowly buried beneath Mesoproterozoic to Quaternary cover sequences. Individual inliers in the Olary Domain form a series of semi-isolated, partly exposed blocks, which characteristically have faulted western margins and are unconformably overlain by Adelaide Rift Complex successions along their eastern margin (Fig. 2). Geological mapping and related investigations in the Olary Domain have been modest in comparison with the extensive and very detailed investigations undertaken around Broken Hill (e.g. Marjoribanks et al., 1980; Brown et al., 1983; Stevens and Stroud, 1983; Stevens, 1986; Stevens and Rothery, 1997; Forbes et al., 2004; Gibson et al., 2004). Most studies of the Curnamona Province have been of limited regional extent except for the syntheses of Campana and King (1958), Grady et al. (1989) and Flint (2002). Descriptions of the geology and mineralisation of the Olary Block often draws extensively on published work from the Broken Hill Domain (see Clarke et al., 2003, and references therein).

Correlations that have been made between the Broken Hill and Olary domains highlight several distinct similarities and differences that have significant implications for tectonic interpretation and metallogenesis (Clarke et al., 1986; Laing, 1995; Page et al., 2000; Leyh and Connor, 2000; Conor, 2004). The Willyama Supergroup is a Palaeo- to Mesoproterozoic package of meta-sedimentary and meta-volcanic rocks that have been interpreted to have been deposited in a intracontinental rift (Willis et al., 1983; Stevens et al., 1988) or a continental back-arc basin (Giles et al., 2002, 2004). The lithostratigraphic nomenclature used in this paper follows that defined by Conor (2004). The Willyama Supergroup is subdivided into lower Curnamona Group and the upper Strathearn Group. These units are characterised by contrasting magnetic susceptibility and composition. The Curnamona Group comprises variably oxidized, magnetite-bearing quartzofeldpathic gneiss, calc-siliacate and calc-albitite gneiss and psammopelitic schist, whereas the overlying Strathearn Group is dominated by pelitic and minor psammitic rocks that are

chemically more reduced and contain varying amounts of graphite.

Between the Curnamona and Strathearn Groups is a major redox boundary that has been interpreted as a stratigraphic horizon termed the Bimba Formation (Conor, 2004) and as an early D1 extensional tectonic contact (Gibson and Nutman, 2004). The Curnamona and Strathearn Groups share a common history of multiple Olarian deformation (D1–D4) and early (M1) low-*P*–high-*T* metamorphism (andalusite-sillimanite facies series) (Hobbs et al., 1984; Gibson, 2000) but have undergone different degrees of partial melting and intrusion by ca. 1710–1670 Ma bimodal magmatic rocks. The Strathearn Group is interpreted as a metamorphic sequence metamorphosed at lower temperatures and at shallower crustal depth than the underlying Curnamona Group. The Strathearn Group is dominated by the prevalence of andalusite rather than sillimanite in M1 mineral assemblage (see Gibson et al., 2004, for review).

Up to four major phases of Olarian deformation have been identified (see Berry et al., 1978; Flint and Parker, 1993). There are differing interpretations of the geometry, orientation and metamorphic conditions under which each event formed. A summary of these different structural evolutionary models (including ours) is presented in Table 1. There is controversy concerning the tectonic context of the first-generation layer-parallel foliation or schistosity (S1) that formed during high-temperature metamorphic conditions. This foliation is typically interpreted as the axial plane structure of regional-scale recumbent folds or nappes with northeast-trending axes (e.g. Clarke et al., 1986). However, F1 fold closures are rarely, if ever, observed in the Strathearn Group. In contrast, post-F1 folds have been reported throughout the Curnamona Group and are usually described as upright to inclined structures with a moderate to steeply dipping axial planar crenulation cleavage. Flint (2002) reported two phases of post-D1 folding, the axial directions of which trended NE and ENE, respectively (D2 and D3 in Table 1).

Berry et al. (1978) reported that the D2 deformation was only weakly developed in the western part of the Olary Domain and did not always develop into a penetrative S2 fabric. The presence of widespread F2 folds was, nevertheless, necessary to explain the geometry and reversals in fold plunge that characterize the younger superimposed D3 structures. In contrast, Clarke et al. (1986) rejected the need for an additional generation of structures between the D1 and D3 deformations of previous investigators (Table 1) and considered the D2 and D3 structures of earlier investigators to be manifestation of the same event (their D2). The D3 deformation of Clarke et al. (1986) was largely restricted to the formation of retrograde shear zones that post-dated the D3 folds of earlier workers.

Based on detailed lithological and structural mapping around the Amerroo Hill area (see Fig. 1), Gibson and Nutman (2004) presented a revised interpretation of the regional structural history, including the high-temperature D1 layer-parallel schistosity. Gibson and Nutman (2004) interpreted that the S1 layer-parallel foliation in the Curnamona Group formed under higher

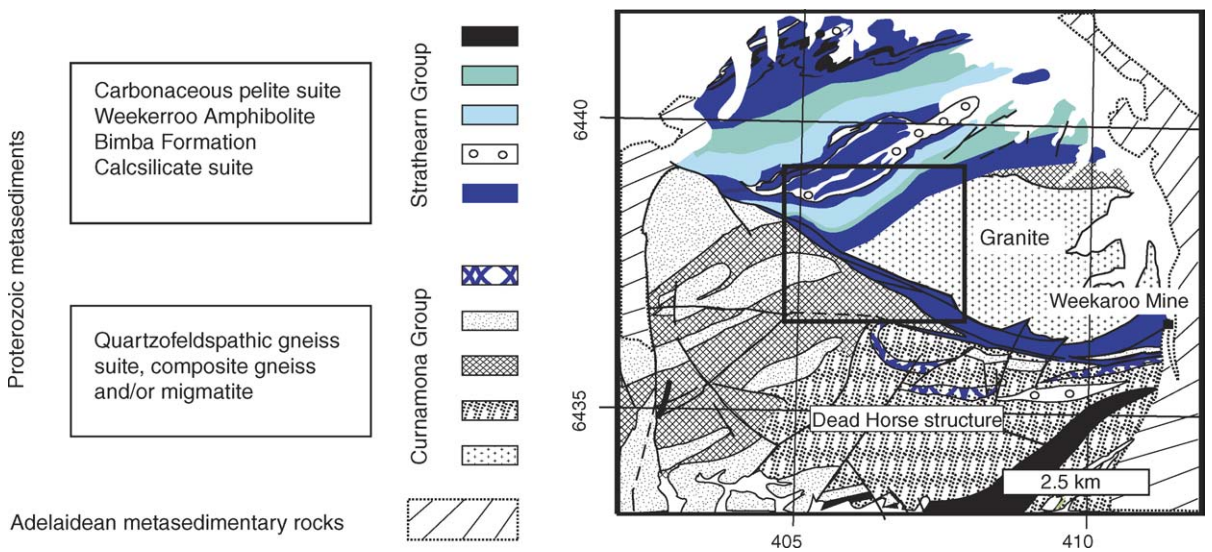

Fig. 3. Simplified geological map of the Weekeroo Inlier (after Laing, 1995; modified). Inset indicates the location of the study area (WOSZ area; Fig. 4).

temperature metamorphic conditions (Table 2) associated with crustal extension of the Curnamona Province. Regional nappes, responsible for widespread overturning of the Willyama Supergroup stratigraphy, were interpreted to have formed during D2 and amphibolite facies conditions. F3 folds post-date peak metamorphism. They occur at all scales, trend NE and are characterised by a moderate to steeply dipping S3 crenulation cleavage. Post-D3 structures trend east to east–northeast and formed under retrograde metamorphic conditions. They include variably plunging kink folds and micaceous oriented shear zones dominated by dip-slip displacement (south-side-up).

We adopt the sequence of deformation events of Gibson and Nutman (2004) because our observation suggest that nappes formed during D2. The origin of the first-generation foliation remain poorly constrained. Our structural investigation focuses on the WOSZ area (see Figs. 3 and 4), which is located along the contact between the migmatite-dominated units of the Curnamona Group and the overlying psammite-pelitic sequence of the Strathearn Group outcrops (i.e., the *redox boundary* of Conor, 2004, and Gibson and Nutman, 2004). The dominant macroscopic structures in the WOSZ area are NE–SW trending upright F3 folds (Bottrill, 1998) within the Strathearn Group. These folds are in contact with a

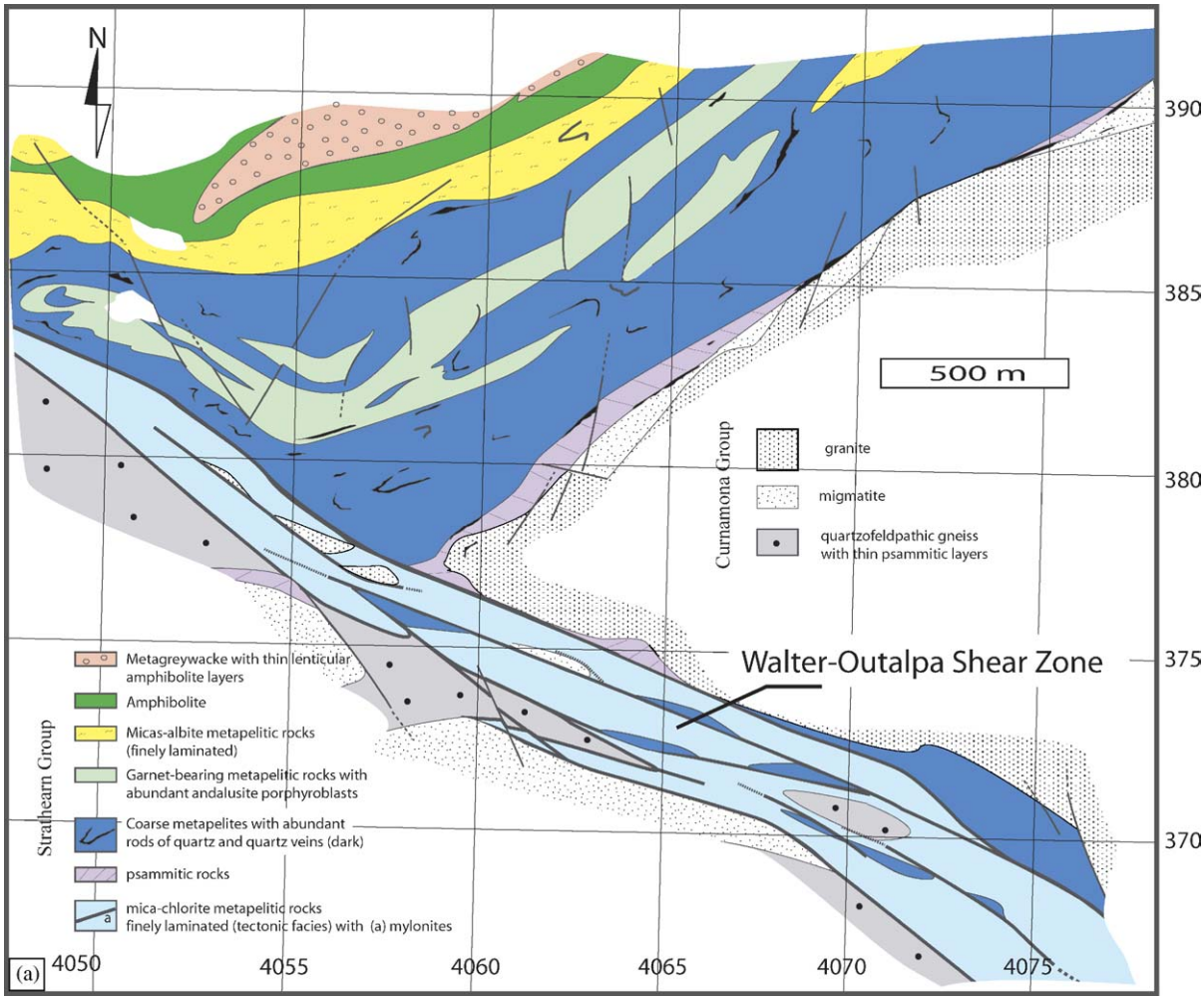

Fig. 4. (a) Map showing distribution of rock types in the WOSZ area. Terminology used for Strathearn Group rocks sequence follows Laing (1995). The distribution of these rocks locally differs from previous mapping by Laing (1995). (b) Structural maps showing the distribution of D2* and D3* structures. Coordinate system used: WGS8. Note in sketch (c) the partitioning of deformation for D3* and ±D2* between the north and the south of the field area. (d) Schematic 3-D block diagrams explaining the relationships between F2 and F3 folds in the north of the field area. In this area, the fold interference patterns vary between (1) domains of complex geometry where the S3 fabric, axial planes of F3 folds, cross-cut at high-angle the axial planes of pre-existing F2 folds; (2) domains of less complex geometry where the axial planes of F2 and F3 folds are nearly parallel.

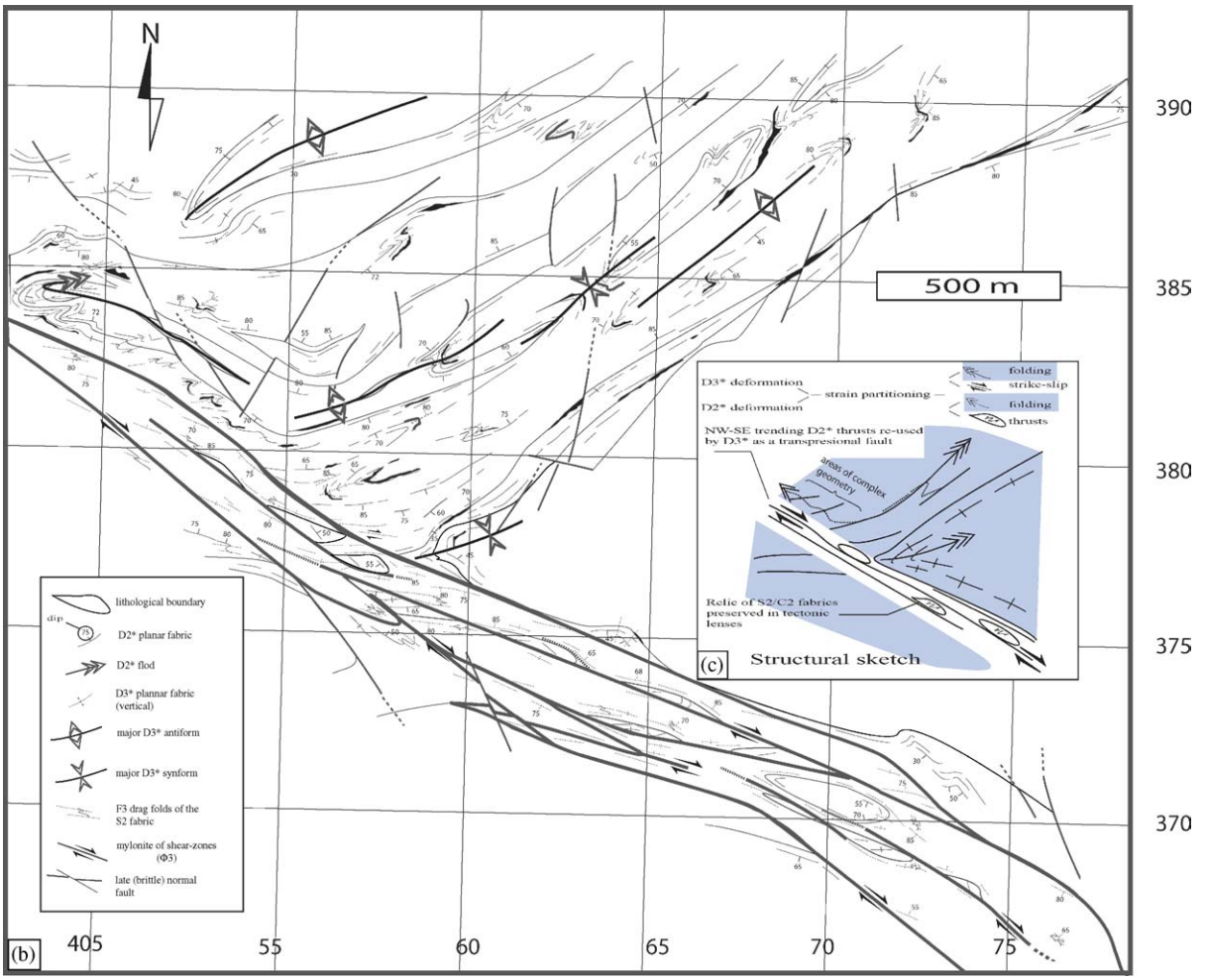

Fig. 4. (*Continued*)

granite pluton, which has been intensely sheared along its southern margin by a kilometre-scale, WNW-trending, D3 WOSZ retrograde shear zone (Hand et al., 2003; Dutch et al., 2005). In this paper, we demonstrate that this shear zone also records thermal conditions and movement history associated with the D2*/M2 tectono-metamorphic events. The "D*" nomenclature is used to relate the different structures to major changes in deformation style or orientation specific to the area around the WOSZ, but not necessarily over the entire Curnamona Province.

4. Deformation and metamorphic history of the WOSZ area

To the north of the WOSZ (Fig. 4a) is a succession of overturned aluminous pelite and psammite units that form part of the Strathearn Group (Laing et al., 1978; Conor, 2004). This sequence is tectonically separated from migmatitic successions of Curnamona Group by the WOSZ. Macro- and mesoscopic structures within the WOSZ area can be described in terms of two main high-strain ductile deformational events (D2* and D3*), with strain progressively partitioned into high-strain zones in the south part of the study area and relatively low-strain areas preserved in the north. The geometry and style of deformation along the WOSZ area is largely due to heterogeneous, non-coaxial flow. Evidence for the D1*/M1 event is poorly preserved within the shear zone.

This study uses the standard techniques of geometric analysis (e.g. Hobbs et al., 1976; Hopgood, 1980; Laajoki and Tuisku, 1990) in conjunction with porphyroblast-matrix microstructural relationship (e.g. Bell et al., 1986; Vernon, 1989; Davis, 1995) to evaluate data from field locations and oriented thin sections.

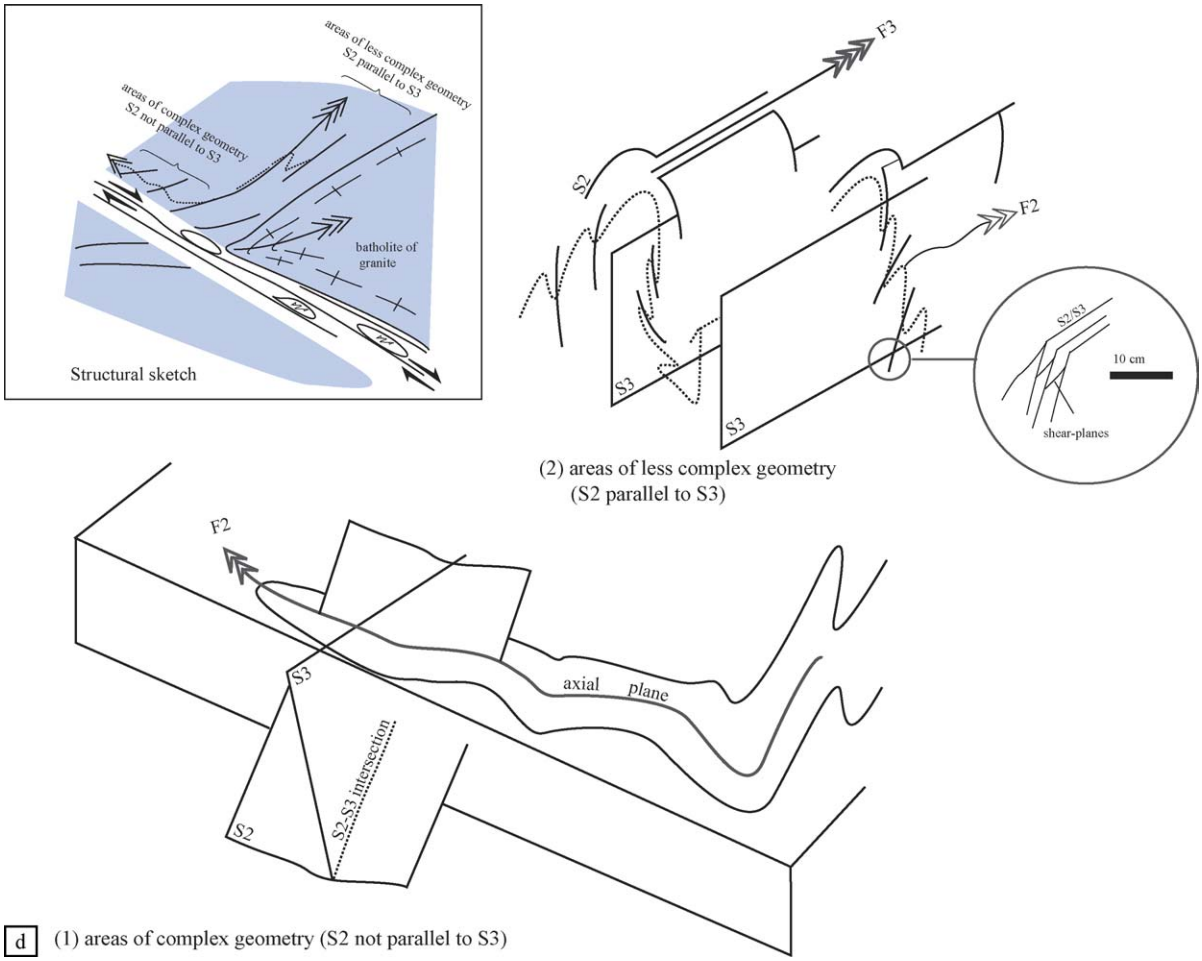

Fig. 4. (*Continued*).

4.1. D1/M1*

The D1* structures and subsequent overprinting relationships is best recorded in the relatively low-strain northern part of the study area and within low-strain areas less effected by the D2* and D3* events. Andalusite-bearing assemblages in the Strathearn Group have been extensively overprinted by subsequent structures related to D2* and D3* but commonly preserve a layer-parallel foliation (S1) defined by muscovite, biotite and oxides (Fig. 5a). This foliation occurs independently of any known folds and is overprinted by porphyroblasts of both potassium feldspar and garnet. Coexisting M1 phases in the meta-pelitic Strathearn Group of the WOSZ area include garnet, andalusite, muscovite, biotite, plagioclase, quartz, ±tourmaline. Small amounts of fibrolite, that are crudely oriented within the S1 fabric and are crenulated during the D2* deformation, may also be part of M1 assemblage but for the most part fibrolite post-date the M1 metamorphism and lies within the S2 foliation (see also Gibson and Nutman, 2004).

4.2. D2/M2 and D3*/M3 in low-strain areas*

Evidence for the D2* deformation is well preserved in D3* low-strain zones, including the Strathearn Group rocks in the north of the WOSZ area. Within the aluminous meta-pelitic rocks, the first recognisable deformation event is D2*. This event is characterised by mesoscopic reclined tight to isoclinal F2 folds. These folds are accompanied by a well-developed bedding/cleavage intersection lineation. A characteristic of this event is the general absence of any associated stretching lineations. The S2 in these areas is folded by a series of upright open F3 folds so that the S2 form surfaces are dominated by SW-trending and steeply NW- and SE-dipping (or vertical) attitudes. The F2 folds and associated intersection lineations are commonly refolded by the F3 folds (see

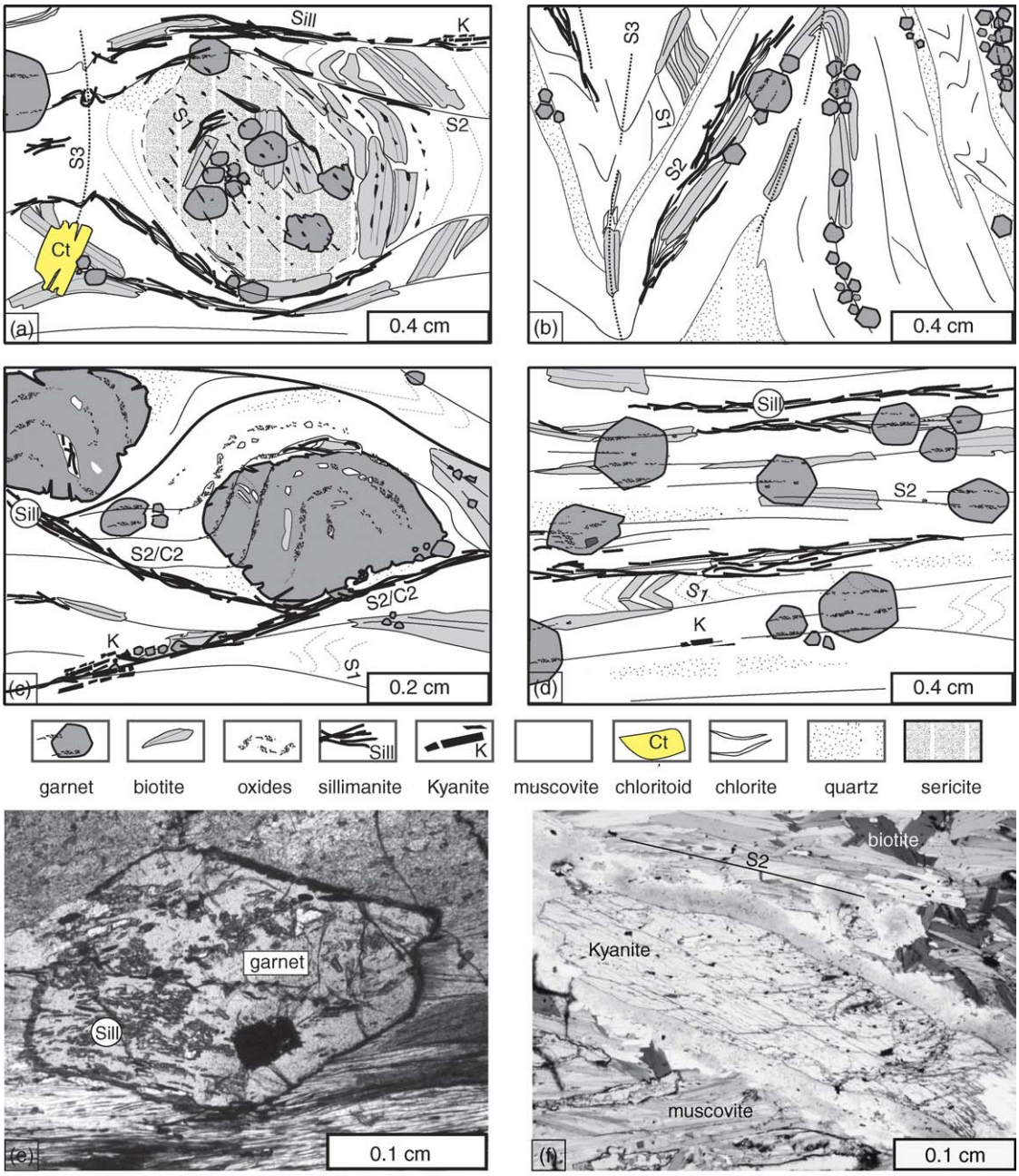

Fig. 5. (a) Pseudomorph of D1*/M1 andalusite porphyroblast with straight S1 fabric defined by biotite and oxides inclusions (dark) whereas same fabrics in rock matrix have been crenulated in between the S2 planes. The crystal of andalusite has been pseudomorphed by a D2*/M2 metamorphic assemblage (i.e., garnet, sillimanite and sericite); note crystal of chloritoid which grow during later D3*/M3 event; it is oriented at high angle with respect to the main S2 fabric of the rock. (b) Discrete S3 crenulation in the hinge of F3 microfolds; the S3 fabric is marked by the growth of chlorite–muscovite–biotite. (c–e) D2* syntectonic garnet porphyroblasts that has overgrown the S2 fabric during general D2/M2 shearing. Note in (c) that the S2 fabric has been strongly crenulated before being incorporated within the garnet porphyroblast. This pattern is characteristic of a strong simple shear at the time of the D2*/M2 event (rock sampled in a D2 tectonic lens within the Walter-Outalpa Shear Zone). This pattern differs from (d and e), where S2 inclusions within garnet porphyroblasts lie parallel to the main S2 fabric of the rock matrix. This rock has been sampled in a D2* low-strain area characterised by dominant flattening. In (c–e), S2 in rock matrix mainly includes biotite, muscovite, fibrous sillimanite as well as flattened aggregates of kyanite (f). (g) Compositional variations of the garnet Clw-27 along the profile A–B (g). This garnet has been sampled in the low-strain area. Note the small bell-shape zoning of Mn and Fe suggesting that the core of this garnet grew during a prograde metamorphism. (h) X-ray map of the same garnet showing that the core has been statically overgrown by a (inferred) D3* garnet generation (Ca-rich rim); relative content of Ca varying from low (dark) to high (white).

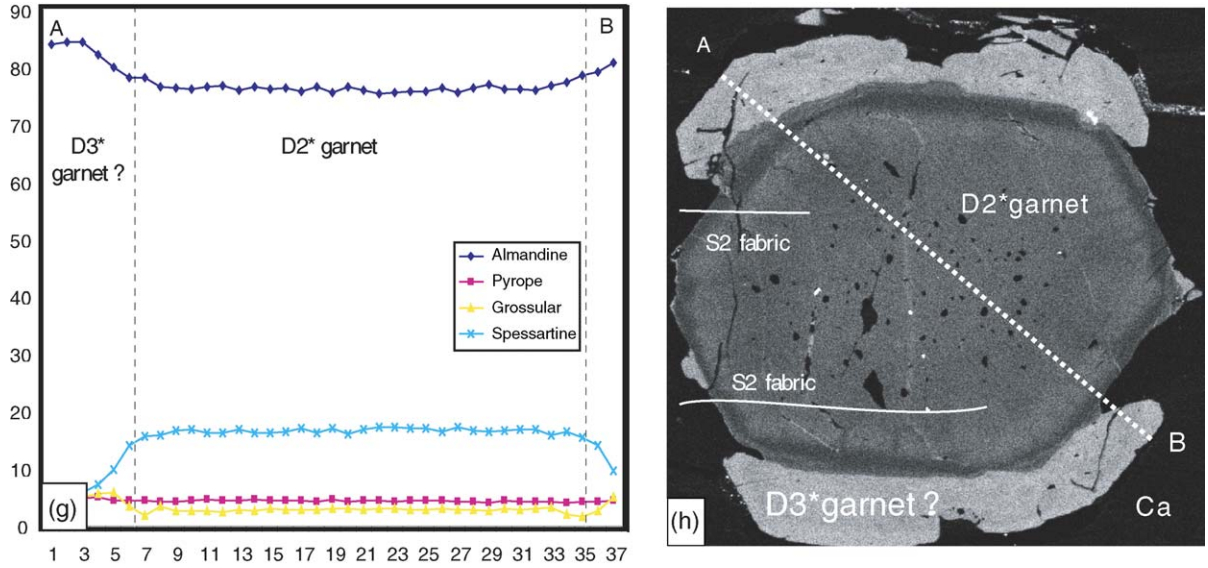

Fig. 5. (*Continued*).

Fig. 6e). Microscopic evidence for a pre-S2 fabric exists in the area, although it cannot be related to an obvious mesoscopic structures. On the basis of geometrical relationships between the D2* and D3* fabrics, we have identified in the north of the WOSZ, in the low-strain zone, two areas characterised by different structural complexity (i.e., the high- and low-complexity areas).

In areas of complex geometry (see Fig. 4c and d), metre- to hundreds of metres-scale tight F2 folds occur in the aluminous meta-pelitic units. The form surfaces of these NW-trending folds mainly follow bounding pegmatite bodies and quartz veins (Fig. 4b), which do not contain this scale of folding. S2 and S3 are not sub-parallel and locally where they are at high angle, S2/S3 intersections plunge between 15° to the N and 27° to the SW. S3 is sub-vertical, indicating that the axial surfaces of F2 folds are steeply dipping. The axial surface to D2* folds were probably originally gently dipping before being steepening by large-scale D3* folds. Such a conclusion is supported by the widespread development of over-turned D2 folds and nappes within the Willyama Supergroup (Clarke et al., 1986; Gibson, 2002; Gibson et al., 2004; Forbes et al., 2004; Forbes and Betts, 2004).

Away from areas of complex geometry, deformation is characterised zones of dominantly planar foliation development. S2 parallel flattening is strong, resulting in the development of centimetre- to metre-scale NE–SW trending F2 recumbent folds (Fig. 4c and d). Locally, the foliation is composite foliation of S2 and S3. In areas where S2 and S3 are sub-parallel there may be the development of extensional shear bands, with horizontal axes, that lie at <25° to the combined foliation. This suggests that the S2/S3 fabric elements have been overprinted by an event in which there was a component of sub-vertical stretching.

In the meta-pelitic unit, sillimanite, muscovite and biotite are the main S2 foliation-forming elements in a typical assemblage of quartz–alkali feldspar–plagioclase and garnet. Straight inclusion trails of the sillimanite foliation suggests that the garnet has overgrown sillimanite (Fig. 5d). Biotite is the main fabric-forming element in the sub-aluminous lithologies in a typical assemblage of quartz–alkali feldspar–plagioclase–biotite ± garnet. In aluminous garnet-bearing rocks within some D2* low-strain areas (where D1* is relatively well-preserved), large (<100 mm) rectangular-shaped andalusite porphyroblasts are pseudomorphed by sillimanite. These porphyroblasts are wrapped around by a S2 sillimanite foliation. This assemblage records earlier D2* conditions and suggests that uppermost amphibolite facies conditions were attained during D2* (at 600 °C and 5–6 kbar according to Clarke et al., 1986), whereas D1* conditions were attained at less than 4 kbar (aluminosilicate triple point) at about 600–650 °C. The occurrence of kyanite–chlorite–muscovite assemblage growing after sillimanite, both in the S2 fabric, suggest that retrograde metamorphism occurred during the waning stages of the D2*/M2 event (see below).

D3*/M3 is characterised by the development of a biotite-muscovite-rich S3 foliation and the development of a prominent chloritoid and chlorite porphyroblasts

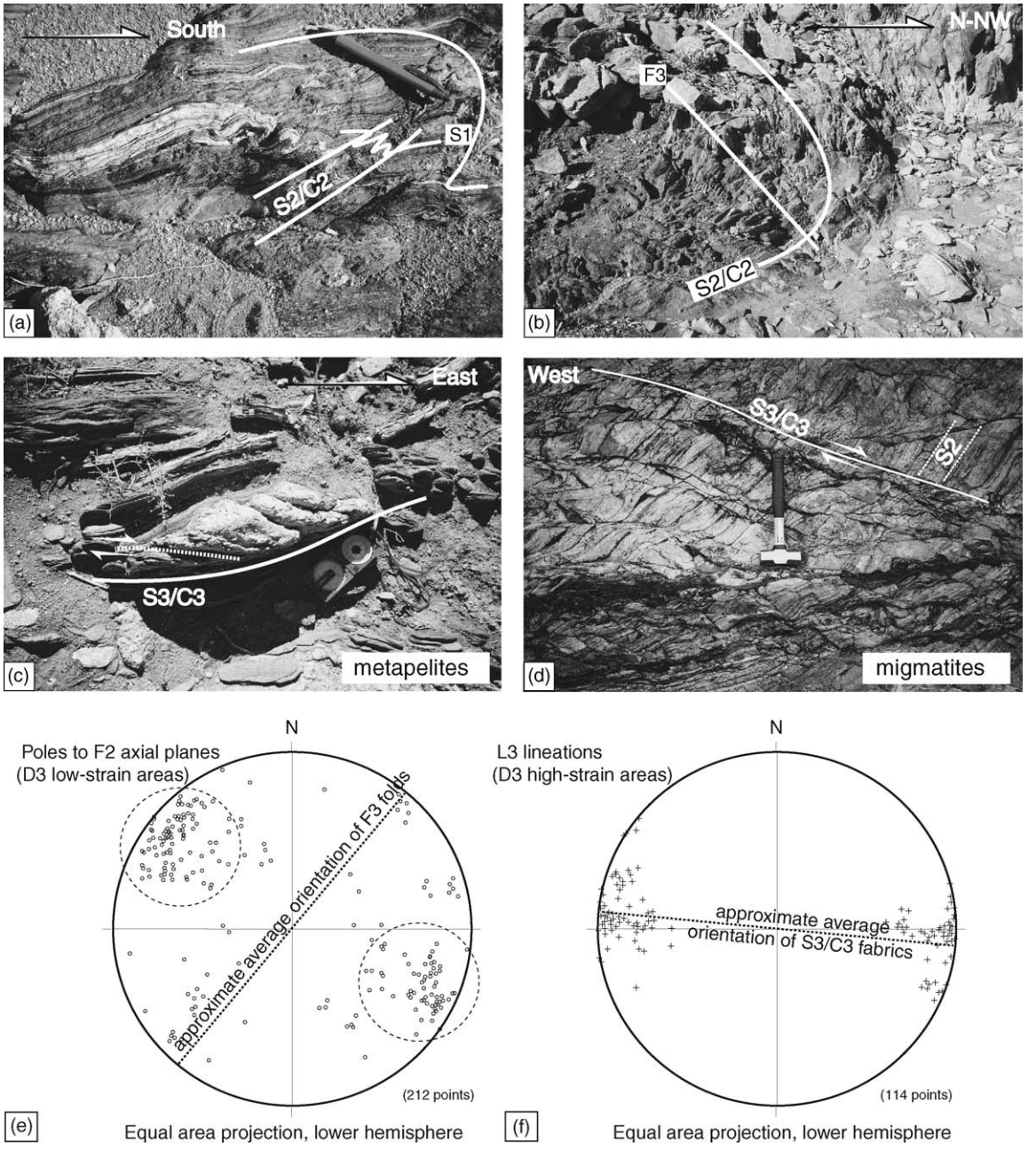

Fig. 6. D2* and D3* ductile deformations in the Walter-Outalpa Shear Zone. (a) F2 isoclinal folds folding the S1 fabric. Two generations of garnet, growing, respectively, in the S1 and S2 fabrics, have been recognised on the field; (b) NE–SW to N–S trending F3 upright-folds bending the S2/C2 fabric. As for (a) this open fold has been observed in a tectonic lens of decametric scale preserving evidence of D2* high-strain shearing. (c and d) Typical examples of pervasive D3* shear zones with top-to-the-east movement direction (dextral movements). An E–W trending lineation is carried by the S3/C3 shear-fabric. (e) Poles to F2 axial planes folded around NE–SW trending F3 folds (low-strain D3* areas) defining two great circles. (f) L3 stretching lineation measured within S3/C3 penetrative shear bands (Walter-Outalpa Shear Zone; high-strain D3* areas).

(Fig. 5a). Most porphyroblasts are idiomorphic and overgrow the muscovite fabric, but the fabric is sometimes flattened around and encloses the porphyroblast (Fig. 8a). The foliation is generally vertical and contains a steeply pitching mineral lineation defined by porphyroblastic aggregates of kyanite, quartz ± garnet (Fig. 5f). Where the M3* assemblages is less strongly developed muscovite replaces S2 sillimanite and gently dipping F3 folds locally develop. Where more strongly developed, a S3 muscovite–biotite NE-trending fabric wraps around

metre-scale lenses of relatively unaffected S2-dominated rocks.

4.3. D2*/M2 and D3*/M3 in high-strain areas

The WOSZ contains two distinct shear-fabric types: (1) a relatively early high-grade fabric (S2/C2); and (2) a later retrograde fabric (S3/C3) that deflects the early fabric. S2/C2 fabrics are preserved in metre- to decametre-scale zones, comparable to residual tectonic lenses, which have been strongly sheared at their boundaries by a network of D3* shear zones.

D2 high-strain zones* are characterised by a combination of foliation and small-scale sillimanite-bearing shear zones. The D2* stage is characterised by well-developed shear planes and by the steeply dipping S2 foliation. Corresponding deformation patterns may be described as ductile syn-foliation S2/C2 shear bands (Berthé et al., 1979), which correspond to Type-I C–S bands of Lister and Snoke (1984). The angle between the C2 and S2 planes is usually low (typically 05°–15°). The S2/C2 is either parallel to axial planes of F2 folds (Fig. 6a) and deforms an earlier S1 foliation, or corresponds to a composite surface resulting from transposition of S1. In the latter case, S1 is preserved in microfolds within S2/C2 defined microlithons. F2 folds axes are sub-horizontal and NW–SE to E–W trending. Shear bands and S2/C2 fish-like structures always indicate a top-to-south movement (north-side-up). A steeply plunging mineral and stretching lineation is ubiquitous on C2 and S2 planes. This lineation is defined by elongated quartz grains or a stretched sillimanite–biotite–muscovite–chlorite fibrous association. Sillimanite is the dominant S2/C2 fabric element in the aluminous meta-pelite units. Nevertheless, the occurrence of kyanite–chlorite–muscovite assemblage growing after sillimanite in the S2/C2 fabric (as a syn-kinematic minerals association) suggests that the D2*/M2 event records a part of retrograde metamorphism. In the sub-aluminous psammitic rocks, biotite is the fabric element in the D2* high-strain zones. In the less-strain D2* zones of meta-pelitic units within the WOSZ, sillimanite occurs as felted mats that are up to 10 mm across. These are intergrown with porphyroblastic biotite. With increasing D2* strain, D1* andalusite and biotite are variably folded as an open crenulation cleavage (Fig. 5a), until a new spaced sillimanite (±kyanite) foliation is developed. This foliation is generally flattened around the garnets, and may be at a high-angle to the D1* inclusion trails of sillimanite within them (Fig. 5a). In the D2* high-strain zones, there is a well-developed fabric, defined by strongly oriented sillimanite or kyanite with *c*-axes parallel to L2 and associated with the biotite–sillimanite–garnet peak metamorphic assemblage that defines the D2* mineral lineation. The sillimanite and kyanite both occurs as large porphyroblasts defining the lineation and as folded mats that enclose garnet. The biotite displays intracrystalline deformation kinked and is partially replaced by the fine sillimanite mats.

D2* high-strain zones can contain F3 folds of various styles: small (mm) to large (m) open to isoclinal disharmonic folds with a characteristic spaced chlorite-rich axial surface cleavage (S3) in the meta-pelitic units (Fig. 6b). Complex superimposed folds are also developed where earlier F2 folds lie oblique to the near vertical east–west-trending S3 foliation, giving Type 2 interference patterns (Ramsay, 1967). Preserved within zones of D2* high-strain are recurring muscovite–chlorite-bearing shear zones that are characterised by an apparently simple planar foliation and a shallow (5°–25°) pitching stretching lineation. These S3/C3 fabrics are associated with sub-horizontal displacements but in some cases, involve vertical offsets that are difficult to evaluate.

D3 high-strain zones* constitute a kilometric-scale network of S3/C3 shear fabrics characterised by a combination of planar foliations, prominent elongation and mineral lineations that trend either to the NE–SW (in the western portion of the study area) or to the ENE to E–W (in the eastern and south portions). These lineations are contained in steep (80°–90°) south dipping foliations (Fig. 4b). Likewise, the mineral or elongation lineation (L3; Fig. 6f) and the F3 parasitic folds are co-linear and consistently plunge shallowly to the east or the west (Fig. 6f). Parasitic folds and asymmetric extensional shear bands indicate that the deformation was in response to dextral, northeast-directed transpression. The Φ3 tectonic contacts mapped on Fig. 4b correspond to strong concentrations of S3/C3 shear bands together with appearance of mylonitic fabrics. In these mylonitic Φ3 zones, the mesoscopic fabric is sometimes defined by transposed layers of various rock-types, strongly interleaved with each other. In the muscovite–garnet-bearing migmatites, the S3/C3 fabric is dominated by a prominent foliation with a strong linear component. Numerous small (10 mm) to large (tens of metres)-scale, tight to isoclinal parasitic folds occur, with axes that are co-linear with the chlorite–staurolite mineral and elongation lineation. In some instances the D3* strain is partitioned around igneous bodies of granite outcropping in the WOSZ. Such bodies are cross-cut by fracture planes (mm spacing) and there is very localised development of S3/C3 fabrics in biotite-rich portions of the shear zones.

These S3/C3 fabrics are associated with sub-horizontal displacements but in some case, involve vertical offsets that are difficult to evaluate.

The D3*/M3 shear event in the WOSZ area may be equivalent to the kyanite- and staurolite-bearing shear zones such as the Thackaringa-Pinnacles shear zone that developed before 1570 Ma (Stevens, 1986), but could be younger, possibly Delamerian structures (Parker, 1972; Dutch et al., 2005). It is noteworthy that the axial traces of the F3 folds on Fig. 4a appear to rotate into parallelism with the shear zone to the north, suggesting that shear zone activity continued late into the D3* deformation or during later deformation events. Structural studies (e.g. Bottrill, 1998) have nevertheless shown that some of the WOSZ are truncated at the base of the Neoproterozoic-aged Adelaide Rift Complex cover successions, and therefore, must predate the deposition of these Neoproterozoic sediments. Nevertheless, in other part of the Curnamona Province, Laing (1969) and Lishmund (1982) showed that many of the so-thought D3 shear zones disrupt the Adelaidean cover sequences.

4.4. D2/M2 and D3*/M3 stain partitioning: insight from high-resolution P–T paths*

In recent years, the estimation of the thermobarometric evolution of metamorphic rocks has been greatly improved. In particular, energy minimizing approaches (De Capitani and Brown, 1987; see also Powell and Holland, 1994) leading to the construction of increasingly more realistic and accurate petrogenetic grids and pseudo-sections grids, which are a powerful tool to constrain *P–T* evolutions. Such petrogenetic grids can effectively predict the evolution of the rock mineralogy as well as the abundance and composition of phases with evolving *P* and *T*, and for a fixed bulk rock composition (e.g. Powell and Holland, 1994 or Meyre et al., 1997). However, these methods have several limitations, such as: (1) the knowledge of the bulk composition of the reacting systems might be different from that of the bulk rock (Marmo et al., 2002); (2) the ability to identify a suite of stable mineral assemblages in the natural samples (some of the early phases may have completely disappeared); and (3) the thermodynamic properties of all end-members and solid solution models for all phases of variable composition must be known precisely. In order to avoid these problems, a complementary approach, such as the multi-equilibrium calculation approach (Berman, 1991, see also Powell and Holland, 1994) can be used. This approach is less sophisticated since it does not predict which minerals are stable for fixed *P*, *T* and system composition. However, it permits the *P–T* equilibrium condition of a given paragenesis to be calculated. Vidal and Parra (2000) illustrated that the multi-equilibrium approach can be used to estimate *P–T* conditions from the composition of co-existing chlorites and phengites. Since then, the thermodynamics of these phases has been reworked (Vidal et al., 2001; Parra et al., 2002) and numerous natural studies indicate that the method has a good potential to constrain a continuous *P–T* evolution for meta-pelitic rocks metamorphosed at $300 < T < 550\,^{\circ}C$ using a limited number of rock samples (e.g. Vidal and Parra, 2000; Trotet et al., 2001a, b; Bosse et al., 2002; Rolland et al., 2003 and Ganne et al., in press). From these studies of natural samples, it appears that:

- At temperatures $<\sim 550\,^{\circ}C$, equilibration of chlorites and phengites with varying pressure and temperature is controlled by crystallization/recrystallization processes rather than by changing the composition of the other grains by lattice diffusion (see Worley et al., 1997). Equilibrium is therefore achieved only locally.
- New grains nucleate in specific parts of rock, the location of which is controlled by the deformation pattern at the microscopic scale. There is a strong link between deformation and the shape and size of the domains in local equilibrium.
- Contrasting *P–T* conditions caused by different local equilibria achieved in different parts of the same thin section and at different times can be calculated from the same thin section.
- The relative time of growth of phyllosilicates can in many instances be determined using microstructural criteria.

Two samples, representative of the high-strain (JG-13) and low-strain zones (Clw-14) were chosen. Their mineral assemblages were analysed to determine the *P–T* conditions prevailing during the D2*/M2 and D3*/M3 events. Samples were analysed on a CAMEBAX SX-50 microprobe, at the University of Melbourne. Counting times were 15–30 s on peak and 5–30 s per element on background depending on concentrations. The accelerating voltage was 15 kV and the beam current 20–25 nA. Natural silicates were used as standards. Only a few selected analyses are given in this paper for reference (Tables 3 and 4). The entire database is available upon request.

JG-13 is a chlorite-bearing schist strongly deformed in a D3* mylonitic shear zone. Thin section analysis indicates that most of the phengitic micas formed during the D3* stage. Several relicts of S2 assemblages preserved as microlithons were also analysed.

Table 3
Chemical composition of chlorites analysed in the D2* and D3* fabrics (sample JG-13)

Fabric	Chlorite sample																						
	JG-13																						
	34-1	62-1	67-1	68-1	69-1	70-1	71-1	72-1	73-1	74-1	75-1	76-1	77-1	78-1	79-1	80-1	22-1	36-1	37-1	50-1	51-1	52-1	54-1
	S3	S3	03	S3	S3	S3	S3	S3	S3	S3	S3	S3	S3	S3	S3	S3	S2	S2	S2	S2	S2	S2	S2
SiO_2	24.43	27.528	26.269	24.245	24.738	24.882	24.537	24.483	25.85	24.118	24.402	24.106	24.806	24.52	24.261	24.681	24.699	24.734	25.037	24.515	23.903	24.652	25.372
TiO_2	0.0428	0.0678	0.0682	0.0602	0.0941	0.0404	0.0584	0.0774	0.0553	0.0875	0.0875	0.0654	0.1034	0.0958	0.1131	0.1004	0.053	0.0959	0.0601	0.0764	0.0888	0.0817	0.0725
Al_2O_3	22.387	24.389	22.51	22.436	22.554	23.129	22.614	22.701	23.381	22.573	22.504	22.578	22.828	22.895	22.616	23.134	22.802	22.957	22.731	22.406	22.611	22.76	22.978
FeO total	24.241	21.646	21.697	23.994	24.269	23.667	23.955	23.901	22.655	23.486	24.018	23.961	23.722	24.441	24.052	24.142	23.748	24.45	24.075	23.859	24.092	23.676	23.958
MnO	0.669	0.5021	0.5152	0.6484	0.5715	0.5019	0.5728	0.5215	0.6098	0.5343	0.64	0.6486	0.5397	0.6423	0.699	0.675	0.5636	0.6242	0.611	0.549	0.5407	0.633	0.5738
MgO	15.22	12.867	13.386	15.385	15.187	15.012	15.645	15.419	13.925	15.269	16.082	15.59	15.342	15.462	15.619	15.639	15.2	15.639	15.02	15.464	15.341	15.183	15.668
CaO	0.0015	0.0082	0.0015	0.0015	0.0018	0.0224	0.0054	0.0236	0.0082	0.0015	0.0126	0.0179	0.0352	0.0015	0.018	0.0015	0.02	0.029	0.0108	0.0015	0.0015	0.0082	0.0015
Na_2O	0.007	0.0574	0.0422	0.0069	0.0194	0.0233	0.0444	0.003	0.0221	0.044	0.0083	0.003	0.0069	0.0031	0.003	0.003	0.0097	0.0167	0.003	0.003	0.0513	0.003	0.0317
K_2O	0.0057	0.0526	0.4353	0.0105	0.0202	0.0259	0.0394	0.0065	0.0098	0.0348	0.0014	0.0014	0.0016	0.0122	0.0014	0.0014	0.0123	0.031	0.0389	0.0153	0.0292	0.0041	0.0057
Cr_2O_3	0.0016	0.0333	0.0016	0.0016	0.0261	0.0326	0.05690	0.0231	0.0016	0.0016	0.0228	0.0195	0.0016	0.0016	0.0426	0.0016	0.0016	0.0132	0.0718	0.013	0.0016	0.0264	0.0131
Total	87.004	87.118	84.924	86.787	87.454	87.304	87.469	87.136	86.516	86.147	87.757	86.972	87.385	88.072	87.382	88.377	87.108	88.576	87.586	86.889	86.658	87.002	88.661
Oxygen	14	14	14	14	14	14	14	14	14	14	14	14	14	14	14	14	14	14	14	14	14	14	14
Si	2.5902	2.832	2.8011	2.5751	2.6051	2.6118	2.5818	2.5837	2.7133	2.5736	2.562	2.5552	2.6046	2.5674	2.5597	2.5691	2.6033	2.5735	2.6269	2.5953	2.5456	2.6018	2.6235
Ti	0.0034	0.0052	0.0055	0.0048	0.0075	0.0032	0.0046	0.0061	0.0044	0.007	0.0069	0.0052	0.0082	0.0075	0.009	0.0079	0.0042	0.0075	0.0047	0.0061	0.0071	0.0065	0.0056
Al	2.7975	2.9572	2.8289	2.8085	2.7992	2.8612	2.8043	2.8234	2.8925	2.8389	2.7846	2.8205	2.8248	2.8253	2.8123	2.8382	2.8325	2.8151	2.8108	2.7956	2.8379	2.8311	2.8003
Al^{iv}	1.4064	1.1627	1.1935	1.4201	1.3875	1.385	1.4136	1.4102	1.2823	1.4194	1.4311	1.4396	1.3873	1.4251	1.4313	1.423	1.3925	1.419	1.3684	1.3986	1.4473	1.3917	1.3708
Al^{vi}	1.3911	1.7944	1.6355	1.3884	1.4117	1.4762	1.3907	1.4132	1.6102	1.4195	1.3535	1.381	1.4375	1.4002	1.381	1.4152	1.44	1.3961	1.4425	1.397	1.3906	1.4393	1.4295
FeT	2.1496	1.8625	1.935	2.1315	2.1375	2.0778	2.1081	2.1096	1.9889	2.0961	2.109	2.1242	2.0832	2.1404	2.1225	2.1019	2.0935	2.1277	2.1127	2.1126	2.1459	2.0899	2.072
Fe^{3+}	0	0	0	0	0	0	0	0	0	0	0	0	0	0	0	0	0	0	0	0	0	0	0
Mn	0.0601	0.0438	0.0465	0.0583	0.051	0.0446	0.051	0.0466	0.0542	0.0483	0.0569	0.0582	0.048	0.057	0.0625	0.0595	0.0503	0.055	0.543	0.0492	0.0488	0.0566	0.0503
Mg	2.4056	1.9734	2.1279	2.436	2.3841	2.3491	2.454	2.4257	2.1789	2.4289	2.5171	2.4635	2.4014	2.4136	2.4568	2.4268	2.3884	2.4257	2.3494	2.4405	2.4356	2.3889	2.4152
Ca	0.0002	0.0009	0.0002	0.0002	0.0002	0.0025	0.0006	0.0027	0.0009	0.0002	0.0014	0.002	0.004	0.0002	0.002	0.0002	0.0023	0.0032	0.0012	0.0002	0.0002	0.0009	0.0002
Na	0.0014	0.0114	0.0087	0.0014	0.004	0.0047	0.0091	0.0006	0.0045	0.0091	0.0017	0.0006	0.0014	0.0006	0.0006	0.0006	0.002	0.0034	0.0006	0.0006	0.0106	0.0006	0.0064
K	0.0008	0.0069	0.0592	0.0014	0.0027	0.0035	0.0049	0.0009	0.0013	0.0047	0.0002	0.0002	0.0002	0.0016	0.0002	0.0002	0.0017	0.0041	0.0052	0.0021	0.004	0.0006	0.0008
R^{2+}	4.6153	3.8796	4.1094	4.6258	4.5726	4.4715	4.6132	4.5818	4.2221	4.5733	4.683	4.6459	4.5326	4.6109	4.6417	4.5882	4.5322	4.6084	4.5164	4.6023	4.6303	4.5354	4.5375
Total	6.0088	5.6933	5.813	6.0173	5.9912	5.9585	6.0185	5.9992	5.839	6.0069	6.0398	6.0297	5.9757	6.0136	6.0256	6.0043	5.9781	6.0152	5.9659	6.0022	6.0356	5.9768	5.9742
Reste	4.6778	3.9426	4.2241	4.6872	4.6304	4.5269	4.6789	4.6326	4.283	4.6356	4.7432	4.707	4.5861	4.6703	4.707	4.6487	4.5884	4.6741	4.5777	4.6544	4.6938	4.5941	4.595
Vac	−0.009	0.3067	0.187	−0.017	0.0088	0.0415	−0.018	0.0008	0.161	−0.007	−0.04	−0.03	0.0243	−0.014	−0.026	−0.004	0.0219	−0.015	0.0341	−0.002	−0.036	0.0232	0.0258
ln (Fe/Mg)	−0.113	−0.058	−0.095	−0.134	−0.109	−0.123	−0.152	−0.14	−0.091	−0.147	−0.177	−0.148	−0.142	−0.12	−0.146	−0.144	−0.132	−0.131	−0.106	−0.144	−0.127	−0.134	−0.153
T (°C) estimates (Jowett. 1991)	394.7	317.4	326.91	398.89	388.68	387.79	396.69	395.69	355.28	398.55	402.07	405	388.36	400.59	402.37	399.75	390.11	398.57	382.61	391.96	407.63	389.85	383.03
X_{Mg}	0.5281	0.5145	0.5237	0.5333	0.5273	0.5306	0.5379	0.5348	0.5228	0.5368	0.5441	0.537	0.5355	0.53	0.5365	0.5359	0.5329	0.5327	0.5265	0.536	0.5316	0.5334	0.5382
Selected analysis for *P–T* estimates (see Fig. 8a)							8	11								12	6	14	13	1	4		15

Abbreviations and parameters used at the bottom of the table are detailed in Vidal and Parra (2000) and Parra et al. (2002).

Table 4
Chemical composition of white micas analysed in the D2* and D3* fabrics (sample JG-13)

Fabric	Phengite sample JG-13																					
	38 S3	39 S3	40 S3	42 S3	83-1 S3	84-1 S3	89-1 S3	91-1 S3	105-1 S3	142-1 S3	150-1 S3	151-1 S3	152-1 S3	153-1 S3	106-1 S2	107-1 S2	108-1 S2	109-1 S2	122-1 S2	127-1 S2	128-1 S2	129-1 S2	132-1 S2
SiO_2	47.349	47.559	47.028	47.019	48.143	47.313	47.876	47.896	47.6	47.37	45.777	46.822	45.694	47.688	47.704	46.837	47.509	48.176	46.75	46.88	47.429	47.638	46.798
TiO_2	0.3446	0.3723	0.3151	0.361	0.4206	0.3601	0.4135	0.3736	0.4221	0.4666	0.4236	0.407	0.3562	0.4927	0.332	0.3696	0.3794	0.3622	0.3031	0.3297	0.3845	0.4247	0.2947
Al_2O_3	35.182	36.179	35.728	37.006	35.615	36.325	35.827	35.638	35.273	36.645	34.797	36.318	34.857	37.866	35.948	35.948	35.911	35.643	35.811	35.532	36.162	35.678	35.914
FeO total	2.8285	2.7183	3.0221	2.7444	3.11	2.773	2.9123	2.8382	3.0002	2.3022	2.9184	2.6329	2.837	1.3882	2.7543	2.816	2.7868	3.0766	2.788	2.9116	2.9381	2.8268	2.7459
MnO	0.7348	0.6899	0.771	0.6153	0.8126	0.6998	0.8024	0.8442	0.8715	0.5828	0.9309	0.5765	0.7266	0.4283	0.7916	0.6774	0.6706	0.7665	0.7106	0.7726	0.7058	0.7367	0.7294
MgO	0.0387	0.0016	0.0028	0.0016	0.0016	0.0016	0.0028	0.028	0.0361	0.0056	0.014	0.0556	0.0166	0.0016	0.036	0.0016	0.0016	0.0016	0.0016	0.0223	0.0166	0.0028	0.0249
CaO	0.0016	0.0133	0.0028	0.0268	0.0016	0.0016	0.0016	0.0058	0.0016	0.0016	0.0016	0.0016	0.0038	0.0016	0.0152	0.0016	0.0016	0.0016	0.0016	0.0016	0.0016	0.0016	0.0016
Na_2O	1.2968	1.072	0.7882	1.2583	0.9907	0.8564	0.6676	1.1385	0.5697	1.1321	0.6576	0.764	1.1633	1.1406	0.9258	1.2827	1.0304	0.9228	1.2422	1.0548	1.2658	1.2053	1.101
K_2O	9.2311	9.012	9.7054	9.1314	9.4381	8.7329	9.7582	9.1425	9.6687	9.4459	9.7873	9.6019	8.8263	9.0833	9.6957	9.2086	9.6191	9.6547	9.2574	9.2681	9.1327	9.0927	9.2051
FeO	1.4143	2.7183	3.0221	2.7444	3.11	2.773	2.9123	2.8382	3.0002	2.3022	2.9184	2.6329	2.837	1.3882	1.3772	2.816	2.7868	3.0766	2.788	2.9116	2.9381	2.8268	2.7459
Fe_2O_3	1.4143	0	0	0	0	0	0	0	0	0	0	0	0	0	1.3772	0	0	0	0	0	0	0	0
F	0	0	1.13	0.531	0.702	0.098	0.098	0.244	0.326	0.424	0.975	0.39	0.39	0.39	0	0	1.13	0.531	0.702	0.098	0.098	0.244	0.326
Total	97.007	9761.7	9736.3	9816.4	9853.3	9706.4	9826.2	9790.5	9744.3	9795.1	9530.7	9718	9448.1	9809	98.202	9714.2	9790.9	9860.5	9686.5	9677.3	9803.6	9760.7	9681.4
Si	3.0999	3.0901	3.0822	3.0443	3.1123	3.085	3.1033	3.1096	3.1127	3.0691	3.0734	3.0639	3.0776	3.059	3.087	3.0698	3.0902	3.1138	3.0736	3.0855	3.078	3.1016	3.0748
Ti	0.017	0.0182	0.0155	0.0176	0.0204	0.0177	0.0202	0.0182	0.0208	0.0227	0.0214	0.02	0.018	0.0238	0.0162	0.0182	0.0186	0.0176	0.015	0.0163	0.0188	0.0208	0.0146
Al	2.7146	2.7704	2.7598	2.8239	2.7135	2.7915	2.7369	2.7269	2.7184	2.7982	2.7534	2.8009	2.7669	2.8626	2.7416	2.7768	2.753	2.7151	2.7748	2.7562	2.7659	2.7377	2.781
Al^{iv}	0.8832	0.8917	0.9022	0.9381	0.8673	0.8974	0.8766	0.8722	0.8665	0.9081	0.9052	0.9161	0.9044	0.9173	0.8969	0.912	0.8912	0.8686	0.9114	0.8982	0.9032	0.8776	0.9107
Al^{vi}	1.8315	1.8787	1.8576	1.8857	1.8463	1.8941	1.8604	1.8548	1.8519	1.8901	1.8482	1.8848	1.8626	1.9454	1.8447	1.8648	1.8618	1.8466	1.8634	1.858	1.8626	1.8601	1.8703
Fe^{2+}	0.0774	0.1477	0.1657	0.1486	0.1682	0.1512	0.1579	0.1541	0.1641	0.1248	0.1639	0.1441	0.1598	0.0745	0.0745	0.1544	0.1516	0.1663	0.1533	0.1603	0.1595	0.1539	0.1509
Fe^{3+}	0.0697	0	0	0	0	0	0	0	0	0	0	0	0	0	0.0671	0	0	0	0	0	0	0	0
Mn	0.0407	0.038	0.0428	0.0337	0.0445	0.0386	0.0441	0.0464	0.0483	0.032	0.0529	0.032	0.0415	0.0233	0.0434	0.0376	0.0369	0.042	0.0396	0.0431	0.0388	0.0406	0.0406
Mg	0.0038	0.0002	0.0003	0.0002	0.0002	0.0002	0.0003	0.0027	0.0035	0.0005	0.0014	0.0054	0.0017	0.0002	0.0035	0.0002	0.0002	0.0002	0.0002	0.0022	0.0016	0.0003	0.0024
Ca	0.0001	0.0009	0.0002	0.0019	0.0001	0.0001	0.0001	0.0004	0.0001	0.0001	0.0001	0.0001	0.0003	0.0001	0.0011	0.0001	0.0001	0.0001	0.0001	0.0001	0.0001	0.0001	0.0001
Na	0.1646	0.135	0.1002	0.158	0.1242	0.1083	0.0839	0.1433	0.0722	0.1422	0.0856	0.0969	0.1519	0.1419	0.1162	0.163	0.1299	0.1156	0.1583	0.1346	0.1593	0.1522	0.1403
K	0.771	0.747	0.8115	0.7542	0.7784	0.7264	0.8069	0.7572	0.8066	0.7808	0.8383	0.8016	0.7584	0.7433	0.8004	0.77	0.7982	0.7961	0.7765	0.7782	0.7561	0.7552	0.7716
Sum oct	2.0231	2.0646	2.0663	2.0682	2.0591	2.0842	2.0626	2.058	2.0678	2.0474	2.0664	2.0663	2.0655	2.0433	2.0332	2.057	2.0505	2.055	2.0565	2.0636	2.0625	2.0549	2.0642
Vac	0.9769	0.9354	0.9337	0.9318	0.9409	0.9158	0.9374	0.942	0.9322	0.9526	0.9336	0.9337	0.9345	0.9567	0.9668	0.943	0.9495	0.945	0.9435	0.9364	0.9375	0.9451	0.9358
Fe + Mg + Mn	0.122	0.1858	0.2087	0.1825	0.2128	0.19	0.2022	0.2032	0.2159	0.1573	0.2182	0.1815	0.2029	0.0979	0.1214	0.1921	0.1887	0.2084	0.193	0.2055	0.1999	0.1948	0.1939
Ox	8.2119	8.1476	8.1859	8.1383	8.1915	8.1256	8.1726	8.2165	8.2235	8.128	8.202	8.208	8.1909	8.0385	8.1932	8.1683	8.1722	8.1968	8.1769	8.2076	8.1887	8.1718	8.1978
Alcalin	0.9357	0.883	0.9119	0.9141	0.9027	0.8348	0.8909	0.901	0.8789	0.9231	0.924	0.8986	0.9106	0.8853	0.9176	0.9331	0.9283	0.9119	0.9349	0.9129	0.9155	0.9075	0.9119
Prl = +1-alcalins	0.0643	0.117	0.0881	0.0859	0.0973	0.1652	0.1091	0.099	0.1211	0.0769	0.076	0.1014	0.0894	0.1147	0.0824	0.0669	0.0717	0.0881	0.0651	0.0871	0.0845	0.0925	0.0881
Tri = +1-vac	0.0231	0.0646	0.0663	0.0682	0.0591	0.0842	0.0626	0.058	0.0678	0.0474	0.0664	0.0663	0.0655	0.0433	0.0332	0.057	0.0505	0.055	0.0565	0.0636	0.0625	0.0549	0.0642
Cel = ($R^{2+} - 3$*tri)	0.0527	−0.008	0.0098	−0.022	0.0355	−0.062	0.0145	0.0292	0.0125	0.0151	0.019	−0.017	0.0065	−0.032	0.0218	0.0212	0.0372	0.0434	0.0236	0.0149	0.0124	0.03	0.0014
Muscovite	0.8368	0.8266	0.8358	0.8686	0.8081	0.8131	0.8139	0.8139	0.7987	0.8606	0.8387	0.8497	0.8387	0.8739	0.8406	0.8549	0.8406	0.8135	0.8549	0.8345	0.8407	0.8226	0.8464
Total	0.9768	1.0003	1.0001	1.0006	1	1	1	1.0001	1	1	1	1	1.0001	1	0.978	1	1	1	1	1	1	1	1
X_K	0.8241	0.8469	0.8901	0.8268	0.8624	0.8703	0.9058	0.8409	0.9178	0.8459	0.9073	0.8921	0.8331	0.8397	0.8733	0.8253	0.86	0.8732	0.8306	0.8525	0.826	0.8323	0.8462
ln (Fe/Mg)	3.0205	6.8598	6.4061	6.8693	6.9944	6.8797	6.3691	4.0408	3.8422	5.4409	4.7618	3.2797	4.5631	6.1878	3.0663	6.8951	6.8847	6.9836	6.8851	4.2939	4.5981	6.3393	4.125
		Ag	R																				
Pa	0.1759	0.1529	0.1098	0.1728	0.1376	0.1297	0.0942	0.1591	0.0822	0.1541	0.0926	0.1079	0.1668	0.1602	0.1266	0.1747	0.14	0.1268	0.1694	0.1474	0.174	0.1677	0.1538
Tri	0.0231	0.0646	0.0663	0.0682	0.0591	0.0842	0.0626	0.058	0.0678	0.0474	0.0664	0.0663	0.0655	0.0433	0.0332	0.057	0.0505	0.055	0.0565	0.0636	0.0625	0.0549	0.0642
TWM	0.0578	0.0572	0.0585	0.0533	0.0651	0.0564	0.0643	0.0651	0.0692	0.0548	0.0744	0.0521	0.0598	0.0472	0.0607	0.0559	0.0556	0.0597	0.0547	0.0595	0.0577	0.0615	0.0553
Ms	0.6327	0.6655	0.7187	0.6985	0.6444	0.6938	0.6982	0.6307	0.6947	0.6767	0.7169	0.7363	0.6603	0.6864	0.6958	0.6634	0.6773	0.6647	0.6726	0.6752	0.6531	0.6279	0.6873
Cel	0.1515	0.0999	0.0898	0.0449	0.1386	0.0748	0.1251	0.1345	0.1347	0.0992	0.1027	0.0696	0.0896	0.0865	0.1295	0.0869	0.1138	0.136	0.0867	0.0977	0.0918	0.1289	0.0803
	97.497	99.895	99.835	99.896	99.908	99.897	99.829	98.272	97.9	99.568	99.152	96.373	98.968	99.795	97.606	99.899	99.898	99.907	99.898	98.653	99.003	99.824	98.409
Selected analysis		8				11						12			6		13	3		10		2	

Abbreviations and parameters used at the bottom of the table are detailed in Vidal and Parra (2000) and Parra et al. (2002).

Clw-14 is a meta-pelite that contains remnant pseudomorphed andalusite porphyroblasts extensively overprinted by D2* and D3* structures. Clw-14 preserves a layer-parallel foliation (S2) defined dominantly by muscovite, chlorite and biotite. Small crudely oriented crystals of kyanite formed after sillimanite and lying within the S2 fabric were crenulated during the D3* deformation. Coexisting M2 phases in the S2 fabric include garnet, plagioclase and quartz. The S2 foliation is axial planar to a metric-scale F2 fold that has been weakly refolded during D3*. S2 is locally overprinted by a discrete fabric (S3) defined by chlorite, muscovite, biotite ± porphyroblastic chloritoid.

4.4.1. Mineral composition

Only analyses conforming to the chemical criteria listed in Vidal and Parra (2000) were retained. These are (1) chlorite analyses showing more than 0.5% ($Na_2O + K_2O + CaO$); mica analyses showing more than 0.5% (MnO + TiO2 + Cl) were rejected; (2) only the compositions that could be expressed as a linear combination of the following end members were retained: (Fe, Mg)-amesite, clinochlorite, daphnite and sudoite for chlorites, and (Fe, Mg)-celadonite, muscovite, paragonite, pyrophyllite and for white micas. Calculation of structural formulae and chemical parameters (as Si^{4+}) for chlorite and white micas follow the Vidal et al. (2001) solid solution models. Structural formulae were calculated on the basis of 14 oxygens for chlorite and 11 for micas. Chlorite in the D2* fabric shows X_{Mg} values ranging from 0.48 to 0.57 and from 0.5 to 0.62 in the D3* fabric (Table 3). These compositional changes probably result from equilibria between chlorite, biotite and white micas (Fig. 7a). Note also in Fig. 7b that these equilibria are controlled by the chemical compositions of the rocks. The maximum celadonite content of white micas ranges from $Si^{4+} = 3.00–3.21$ and X_{Fe} values vary from 0.85 to 0.95 (Table 4). Following the classification of Rieder et al. (1998), such micas range in between the chemical domains of muscovite and phengite. A general term of 'phengite' has been chosen in this paper. The most substituted phengites were found in the D2* fabric. Their Si^{4+} contents ranges from 3.04 to 3.19. Syn-kinematic phengites, with $3.05 < Si^{4+} < 3.21$, that define the two fabrics (S1 and S2) are sometimes interlayered with biotite and paragonite. The phengites associated with the D3* shear zones are characterised by very low-Si^{4+} contents ($3.00 < Si^{4+} < 3.1$).

4.4.2. P–T estimates

Preliminary temperature estimates obtained with the empirical geothermometer of Jowett (1991) show the

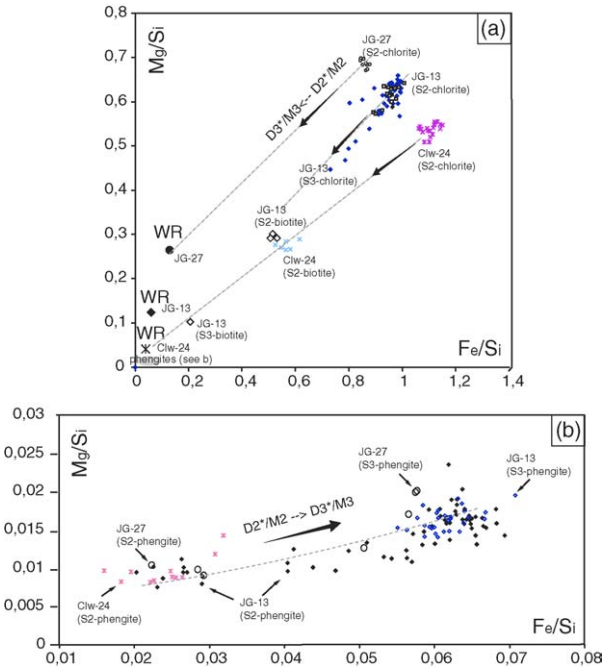

Fig. 7. Compositional variations of the S2 and S3 chlorites, phengites and biotite in a Mg/Si vs. Fe/Si diagram. Samples Clw-14 and JG-13 are described in the text. JG-27 has been sampled in a D2 tectonic lens of micashist within the Walter-Outalpa Shear Zone (see Fig. 5c). (a) Note the chemical equilibrium of the chlorite–phengite–biotite assemblage along the Mg/Fe vector (dotted grey line) with depletion of Mg and Fe for chlorite during the D3*/M3 retrograde metamorphic event (black arrow). This chemical depletion is correlatively associated to an increase of Mg and Fe in S3-phengites. WR: whole rock analysis.

D2* and D3* chlorite–phengite in equilibria at approximately 400 °C (Table 3). More accurate calculations were performed with the TWEEQ and Intersx softwares (Berman, 1991), assuming a water activity equal to unity. Following this procedure, *P–T* estimates for the albite–chlorite–white micas and quartz paragenesis were calculated. Among the initial set of analyses, we only retained those corresponding to chlorite–white micas pairs in contact, in apparent equilibrium (habit and texture), involved in the same microstructures and interpreted to have crystallized at the same time. A further selection of the analyses was made on the basis of the chemical criteria detailed in Vidal and Parra (2000) aimed at rejecting contaminated analyses. The error bars on Fig. 8a and b are proportional to the scattering of the intersection points among all the equilibria that can be calculated from the five-components solid solution model for chlorite and from the six-component model for K-white mica (see Berman, 1991; Vidal and Parra, 2000 for details). The uncertainty on the *P–T* estimates is

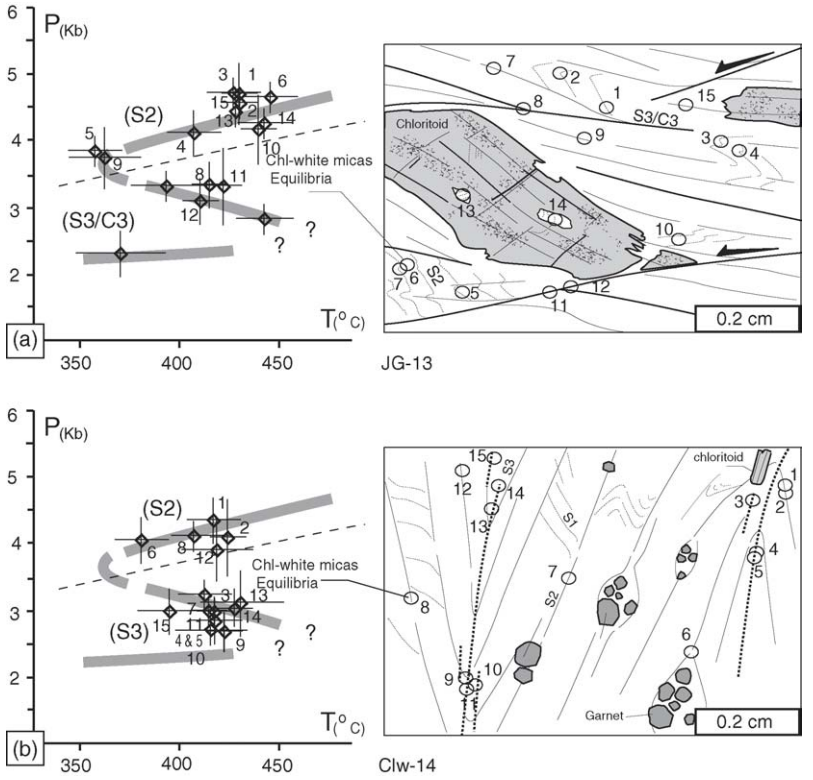

Fig. 8. Proposed *P–T* paths for the D2*/M2 and D3*/M3 events. Tweeq estimates performed on retrograde D2* and D3* chlorite–mica assemblages, and taking into account real mineralogical composition (see chemical analysis; Tables 3 and 4), are presented on the two other grids (a and b). The *P–T* paths corresponding, respectively, to D2*/M2 (post-peak of metamorphism) and D3*/M3 retrograde events in the high-strain (JG-13, a) and low-strain areas (Clw-14, b) are strongly consistent. They suggest for the D2*/M2 event a cooling decompression followed by heating at decreasing pressure during D3*/M3. This is additional evidence to link D2* and D3* simple shears fabrics observed in the south of the WOSZ area with D2* and D3* folds and related-planar fabrics observed in the north. The similar *P–T* evolution proofs that the structural evolution of the WOSZ area has been dominated by strain-partitioning during the two events.

probably less than 1 kbar, 30 °C (Vidal and Parra, 2000; Trotet et al., 2001a).

4.4.3. P–T path

As a whole, the results obtained sample JG-13 and Clw-14 are in good agreement. They suggest for the D2*/M2 event a near-isobaric decompression followed by heating at decreasing pressure during D3*/M3. This peak of temperature at the time of the D3*/M3 event is consistent with the observations of Wilson and Powell (2001) for the Southern Cross area (Broken Hill Domain). Unexpectedly, some D2* and D3* assemblages yielded small different pressure and/or temperature estimates with respect to the retrograde *P–T* path (see Fig. 8b). This discrepancy may indicate either:

(i) the selected phases used for the calculation are not in equilibrium;
(ii) available thermodynamic data are not well-constrained for the considered mineral assemblage;
(iii) the mineral compositions used for the calculation do not record the stable composition because the mineral have been re-equilibrated by diffusion during the retrograde *P–T* path (it may be the case for sample Clw-14).

5. Discussion

5.1. Tectono-metamorphic evolution of the WOSZ area

Progressive localisation of strain within the high-grade rocks in the southwestern part of the Willyama Supergroup has resulted in the formation of a kilometric-scale shear zone (WOSZ) of highly strained D2* and D3* fabrics, separated by less strained zones (Figs. 4b and 9).

In the high-strain zones, D2* and D3* form sub-planar and anastomosing networks of apparently simple S–L tectonite fabrics associated with sub-vertical shearing for D2* (north-side-up) and sub-horizontal shearing

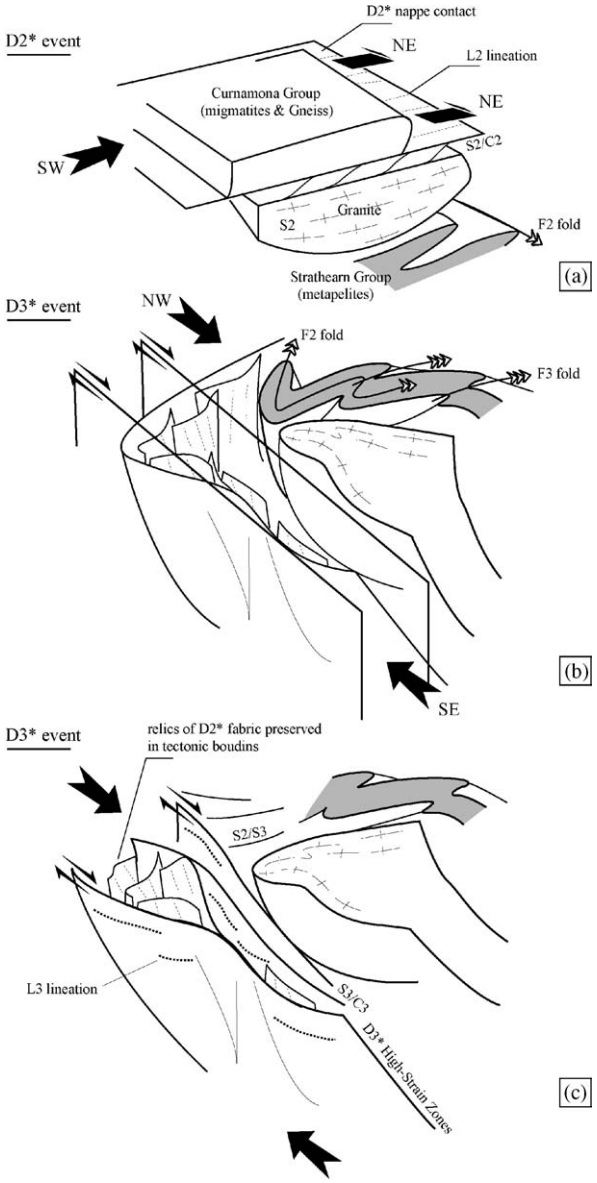

Fig. 9. Sketchs of the tectonic evolution of the WOSZ area showing inversion of original D2* likely-nappe geometry by structures of D3* age. (a) The D2* nappe-forming event was originally partitioned between simple shear (related-thrusts) and flattening; the vergence of the D2* thrusting was probably toward the NW, as discussed by previous authors (see text). (b and c) Evolution of the D2*-nappes refolding during the D3* event. Note the re-using of the D2*-nappe contact as a D3* transpressional tectonic feature.

for D3* (transpressive dextral movements). D3* strike-slip movements are localised in sites of pre-existing D2* high strain. In contrast low-strain zones preserve important folds and flattening foliations associated with both D2* and D3*. In these areas there are complex fold interference patterns; however, early D2* north-side-up dip-slip displacement and recumbent folds are preserved.

The D2*/M2 event is characterised by the growth of biotite–sillimanite–quartz–muscovite–plagioclase–Kf with garnet in meta-pelites, formed at about 600 °C and 5–6 kb (Clarke et al., 1986). D2*/M2 was coeval with the peak metamorphic conditions within the Strathearn Group. The occurrence of kyanite–chlorite–muscovite assemblage after sillimanite in the S2 fabric suggest that the D2*/M2 peak of metamorphism has been followed by a stage of retrograde metamorphism enhanced by the retrograde D3*/M3. D3*/M3 is characterised by the growth of chloritoid–muscovite–chlorite ± staurolite across a muscovite fabric at about 450 °C at 3–4 kb.

We have shown that the kinematic of each separate deformation phase D2* and D3* was the same in areas of high and low strain from which we infer that the structures correspond to the same two events. *P–T* paths established in the high- and low-strain zones of the WOSZ area are also similar (Fig. 8a and b). This similarity further supports the conclusion that D2* and D3* structures preserved in the WOSZ in the south are related to those in the low-strain domain in the north (i.e., fold developments).

5.2. High-strain shear zones: strike-slip or thrusts

It has previously been recognised that high-grade shear zones (Gustafson et al., 1950) disrupt the Curnamona stratigraphy and it was the later work, stimulated by Hobbs et al. (1984) that identified fold style changes across majors shears (Marjoribanks et al., 1980). Many of the shear zones are regarded as being associated with thrusting of the sequence (Marjoribanks et al., 1980; Hobbs et al., 1984; White et al., 1995; Gibson et al., 2004, Gibson and Nutman, 2004; Forbes et al., 2004; Forbes and Betts, 2004). The structural model of Clarke et al. (1986) suggests a series of major north–east trending D2 nappes accompanied the high-grade metamorphism, which were refolded by upright D3 folds. The stratigraphic and structural mapping of Gibson (2002), in different portions of the Willyama Supergroup in the Olary Domain, has produced strong evidence to support the existence of such nappes. However, Wilson and Powell (2001) challenged the interpretation of high-grade D2 structures and reinterpreted the Broken Hill Block as a series of discrete D1 packages, separated from their neighbours by high-angle D2 strike-slip faults.

The results presented here suggest that deformation in the WOSZ included both, an early D2*phase where high-strain zones accommodated thrust/nappes development, and a later D3* phase where earlier formed thrusts were

reactivated as strike-slip faults (Fig. 9). The WOSZ area has been intensively deformed by a heterogeneous D2* nappe-forming event, involving a combination of simple shearing (thrusting) and orthogonal pure shear (flattening). This accounts for the development of a strong planar foliation in the low-strain areas and the S2/C2 shear-fabrics in the high-strain areas. The D2* nappe-forming event has been followed by a D3* heterogeneous transpression, similar to that described by Tikoff and Greene (1997), involving a combination of simple and pure shear. This accounts for the steeply plunging stretching L3 in the low-strain areas and shallow-plunging stretching L3 in the high-strain areas (Fig. 6f).

5.3. The role of lithological variation and pre-existing structures in the partitioning of D2 and D3 strain

5.3.1. Large-scale partitioning

The partitioning of D2* strains into the WOSZ area is clearly controlled by the distribution of rocks types. The zones of non-coaxial strain, in which there is a well-developed S2/C2 fabric, occur along the contact between the migmatites and igneous rocks of the Curnamona Group and the psammite-pelitic units of the Strathearn Group. In this area, this boundary is likely to be linked to a D2* thrust rather than to an early D1* extensional detachment, although it is possible that the contact may have an earlier history such as that described by Gibson and Nutman (2004). This litho-tectonic feature (D2*) later controlled the partitioning of D3* strains. The orientation of D2 NW-trending thrusts coincide with the direction of maximum shearing during D3* strain, explaining its reactivation during D3* as a transpressional fault.

5.3.2. Small scale

Lithological variation within the WOSZ appear to have controlled strain partitioning and localization at all scales (e.g. Bell et al., 1986; Alsop, 1994). The finely laminar nature of the pelitic schist horizon in the study area was important for accommodating large components of progressive shear strain, particularly during reactivation. A consequence of this seems to be the preservation of lenses of D2* shear fabrics in the WOSZ, which elsewhere has been obliterated by D3*. The reason for the preservation of these lenses in different parts of the D3* shear system is probably a result of rheological contrasts between the migmatite-bearing areas in the south and the predominantly aluminous pelite- and/or psammite-rich metasedimentary rocks dominated areas in the north. This partitioning of the strain during D2* and D3* may be applicable to other regions in the Curnamona Province.

5.4. Inferred the age of deformations in the WOSZ area: Olarian or Delamerian?

The high-grade metamorphism and phase of pervasive deformation (D2*/M2) are ascribed to the D2 Mesoproterozoic Olarian Orogeny that occurred in the Curnamona Province between ca. 1600 and 1590 Ma (Page et al., 2000). The context of the D3*/M3 shearing event is more subjective given the results of recent Sm–Nd isotopic analysis that yield Cambrian ages for a large number of so-thought D3 shear zones in the Curnamona Province, including the WOSZ (Dutch et al., 2005). These ages contradict interpretations of previous studies (e.g. Rutland and Etherridge, 1975; Glen et al., 1977; Laing et al., 1978; Corbett and Phillips, 1981; Clarke et al., 1986) in which the amphibolite-to-greenschist grade shear zones formed during the retrograde metamorphism associated with the waning stages of the Olarian Orogeny, although numerous workers have proposed that a substantial part of the retrograde reworking of D1 and D2 structures in the Curnamona Province might be associated with the Cambrian aged (ca. 510–490) Delamerian Orogeny (e.g. Berry et al., 1978; Flint and Parker, 1993) and that different generations of retrograde shear zones (D3–D5) could exist in this Province. Nevertheless, in the case of the WOSZ this latter interpretation is supported by the truncation of the shear zone by the basal unconformity to the Adelaide Rift Complex.

Conjecture about the timing of movement along these D3 shear zones is further fuelled by differences in the relative timing of the emplacement of ca. 1590–1580 Ma granite suites with respect to movement along retrograde shear zones (e.g. Page et al., 2003 or Gibson et al., 2004). In our study area, movement along the WOSZ post-dates late-orogenic pluton emplacement (e.g. ca. 1580 Ma Bimbowrie Suite) (Page et al., 2003). This overprinting relationship occurs at several locations throughout the Olary Domain (Noble et al., 2004; Fry and Betts, 2004). In the Broken Hill Domain, the ca. 1590 Ma Mundi Mundi granites are interpreted to have been emplaced after the retrograde D3/M3 event (see works of Gibson et al., 2004 for review). Foliations in these granites are thus interpreted to be Delamerian in age (see Page et al., 2000; Gibson et al., 2004). From these observations, we conclude that either there may be several generations of retrograde shear zone, which have been mistakenly interpreted to belong to the same generation, or that movement along these shear zones occurred coincidently

with ca. 1590–1580 granite emplacement resulting in local variations in overprinting relationships.

Despite the evidence that supports activity along these D3 shear zones during the Olarian Orogeny, the recent Cambrian ages attained from these shear zones (Dutch et al., 2005) must also be reconciled. It is likely that part of the D3*/M3 shear deformation along the WOSZ occurred during the Cambrian, and thus, is designed as D4* in our deformation chronology. Given the structural and metamorphic link that we have established between folds and shear fabrics in the WOSZ area, the Cambrian ages are strongly suggestive of (but do not definitively prove) the upright D3* folds may also have a Cambrian Origin. However, we are cautious of this interpretation because of the likelihood that D4* deformation reactivated the D3* folds rather than was responsible for their

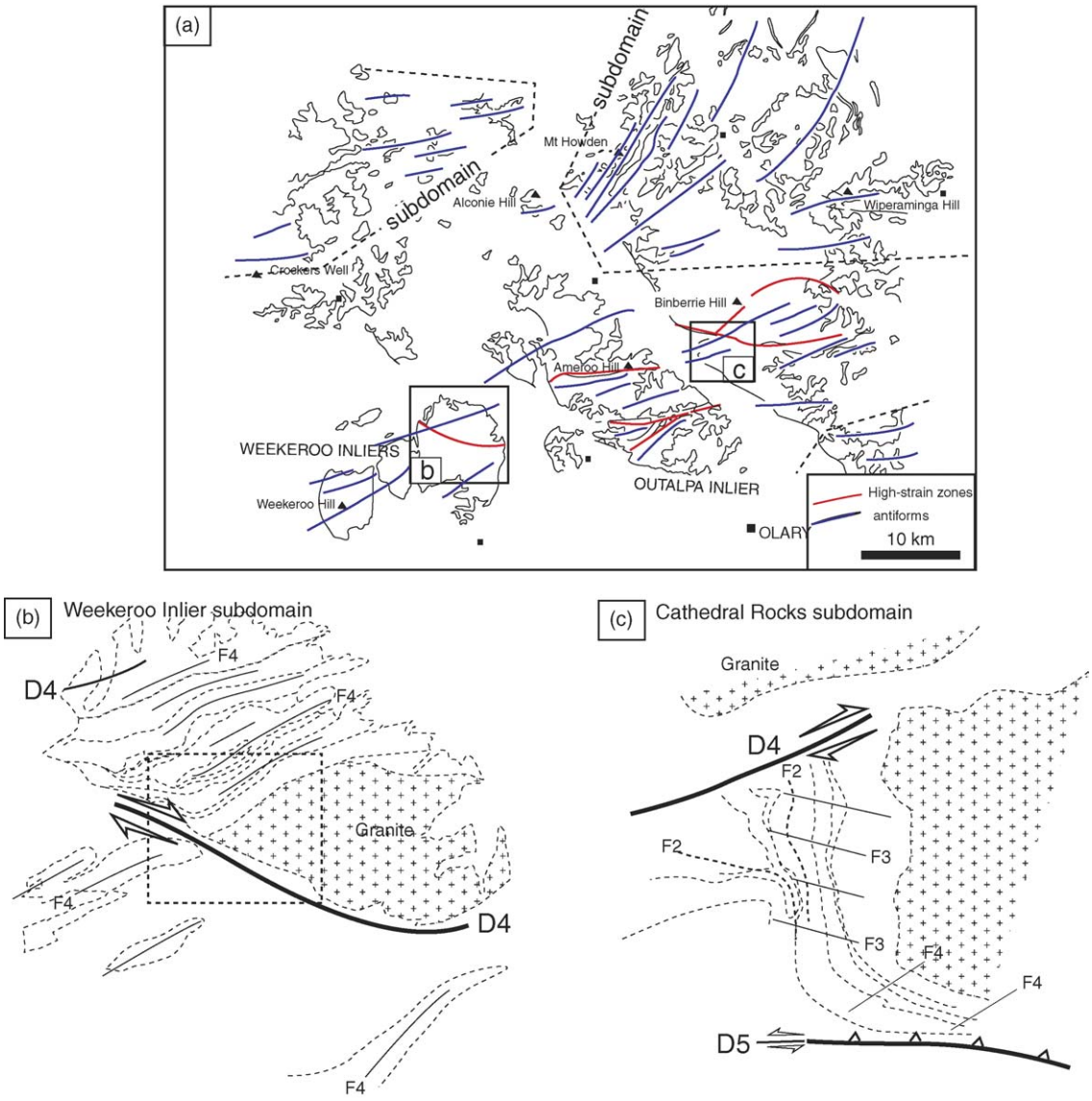

Fig. 10. (a) Structural map of the Olary Domain (Curnamona Province) showing the distribution of (D3*) D4 large-scale structures (i.e. high-strain zones and antiforms trends) (after Clarke et al., 1986; modified). Note the difference in orientation between D4 large-scale structures in this Domain, that led us to define different structural subdomain (see text). (b) Schematic structural map of the Weekeroo Inlier subdomain. Note the difference in orientation between the two majors (D3*) D4 high-strain zones. A domain of D3 low-strain is located in between. The black box corresponds to the WOSZ area. (c) Schematic structural map of the Cathedral Rocks subdomain (after Noble et al., 2004). Observe the youngest generation of D5 shear-zone (north-side-up) cross-cutting through the (D3*) D4 structures (high-strain zones and folds trending).

formation. Nevertheless, the recent age data of Dutch et al. (2005), together with our structural and metamorphic data, imply the presence of a strong Delamerian overprint (D4), either on fold or shear structures, across substantial tracts of the Curnamona Province.

5.5. Structural evolution of the (D3*) D4 high-strain zones in the Curnamona Province

The WOSZ records a complex structural history, which we have subdivided into two main 'events'. The first clearly recognisable phase of deformation resulted in the formation of a planar compositional fabric and subparallel foliation (S2/C2). S2/C2 is strongly overprinted by another (D3*)/D4* deformation, which is the major deformation phase to affect the WOSZ. The (D3*)/D4* resulted in the extensive reorientation of D2* structures and the formation of a composite S2/S3 shear-fabric. (D3*)/D4* was an extensive high-strain deformation that resulted in the formation of mylonitic rocks throughout the study area. However, at the scale of the Olary Domain (Curnamona Province), retrograde shear sense indicators and associated axial planes of large-scale folds show a marked variation, that enable the definition of different structural sub-domains (Fig. 10a).

These sub-domains represent packages of rocks that have different D4 principal stretching axis orientations or record different senses of shear. The relationship between these different domains is unclear and is often masked by later localised deformation at greenschist facies conditions (Fry and Betts, 2004). In some cases the variation of D4 principal stretching axis appears to be the result of subsequent reorientation of D4 by large-scale folds (e.g., the D5 Delamerian phases of Gibson, 2002) and/or shear reworking (Fig. 10c). In other cases, such as for the WOSZ area, (D3*)/D4* high-strain zones orientation is the result of strain partitioning into early formed weakness zones (Fig. 10b).

6. Conclusions

1. High-strain D2* and D3* phases are the major mesoscopic shearing events in the WOSZ area and are excellently displayed along the contact between the psammite-pelite units of the Strathearn Group and the early migmatites and igneous bodies of the Curnamona Group (the *Redox boundary* of Gibson and Nutman, 2004) which localizes shearing. These high-strain zones are dominated by an S2/C2 and/or S3/C3 fabric with a prominent mineral or elongation lineation (L2 or L3), which have generally obliterated S1 and bedding.
2. Migmatites and igneous bodies of the Curnamona Group in the south reacted rigidly, localising zones of D2* and D3* high strain, to the contact with softer rocks of the Strathearn Group.
3. D2* deformation of the WOSZ area is partitioned between thrusting- and flattening (±folding)-related nappe formation. Thrusts are recorded in high-strain zones, with a sub-vertical extension direction along the contacts of the Curnamona and Strathearn Groups. Flattening is recorded elsewhere in D2* low-strain zones, associated with S2 flattening cleavage and gently plunging fold axes.
4. D3* deformation is partitioned between strike-slip shearing and folding. Strike-slip is focused into high-strain zones along the WOSZ, re-using a pre-existing Olarian D2* thrust. D2* high-strain features have, thus, been partly reactivated by Late Olarian and possibly Delamerian high-strain features. Dextral shearing on the WNW-trending fault suggests a NW–SE maximum shortening axis.
5. D3* high-strain zones in the Curnamona Province are discontinuous strands (Hobbs et al., 1984, see also Wilson and Powell, 2001), and include relicts of D2* higher-grade assemblages not entirely overprinted by (D3*) retrograde assemblages. The extensive retrogression to greenschist facies assemblages of the high-strain zones indicates H_2O addition during shearing, probably accompanying later tectonic exhumation.
6. At a regional scale, the geometry of equivalent shear zones to the WOSZ is variable and has different shear directions defining different structural domains in the Curnamona Province. This reflects, in part, modification by later greenschist facies structures (D5) but more significantly it also reflects the spatial and temporal strain localisation during D4 controlled by early-formed D1 and D2 lithotectonic features.

Acknowledgements

J.G. is grateful to S. Reddy for his encouraging advice, critical reading and constructive discussions on 'shear zone' mechanisms. The authors also wish to thank Ian Fitzsimons for his throughout and extremely constructive review, as well as an anonymous reviewer. This study was funded by the ARC Linkage Grant LP0347807 (P. Betts and W. Preiss) and Pmd-CRC programs (R. Weinberg). We would also like to acknowledge the fruitful discussions with David Giles, Wolfgang Preiss, Andy Burtt and Stuart Robertson on the geology of the Olary Domain.

References

Alsop, G.I., 1994. Relationships between distributed and localized shear in the tectonic evolution of a Caledonian fold and thrust zone, northwest Ireland. Geol. Mag. 131, 123–136.

Archibald, N., 1980. Old Boolcoomata-Mount Mulga Mine area outcrop geology (1:10 000 geological map). In: Robinson, P.C. (Ed.), Mulga Dam exploration licence 416, final report. South Australia, Department of Mine and Energy. Open file Envelope, 3360 (plan 3360-11; unpublished).

Bailey, C., Eyster, E., 2003. General shear deformation in the Pinaleño Mountains metamorphic core complex. Arizona J. Struct. Geol. 25 (11), 1883–1892.

Bell, T.H., 1981. Foliation development: the contribution geometry and significance of progressive bulk inhomogeneous shortening. Tectonophysics 75, 273–296.

Bell, T.H., Rubenach, M.J., Fleming, P.D., 1986. Porphyroblast nucleation, growth and dissolution in regional metamorphic rocks as a function of deformation partitioning during foliation development. J. Metamorph. Geol. 4, 37–67.

Berman, R.G., 1991. Thermobarometry using multi-equilibrium calculations: a new technique, with petrological applications. Can. Mineral. 29, 833–855.

Berry, R.F., Flint, R.B., Grady, A.E., 1978. Deformational history of the Outalpa area and its application to the Olary Province, South Australia. R. Soc. S. Aust. Trans. 102, 43–54.

Berthé, D., Choukroune, P., Jégouzo, P., 1979. Orthogneiss, mylonite and non coaxial deformation of granites: the example of the South Armorican Shear Zone. J. Struct. Geol. 1, 31–42.

Betts, P., Giles, D., Lister, G.S., Frick, L.R., 2002. Evolution of the Australian lithosphere. Aust. J. Earth Sci. 49, 661–695.

Bosse, V., Ballèvre, M., Vidal, O., 2002. The garnet isograd in the blueschist-facies metapelites of the Ile de Groix (Armorican Massif, France): a record of ductile thrusting during exhumation. J. Petrol. 43, 485–510.

Bottrill, A.N., 1998. Structural and geochronological analysis of the Walter-Outalpa retrograde shear zone in the eastern Weekeroo Inlier. Olary Domain, South Australia. Honours Thesis, University of Adelaide, unpublished.

Brown, R.E., Stevens, B.P.J., Willis, I.L., Stroud, W.J., Bradley, G.M., Barnes, R.G., 1983. Quartzo-feldspathic rocks. In: Stevens, B.P.J., Stroud, W.J. (Eds.), Rocks of the Broken Hill Block: their classification, nature, stratigraphic distribution and origin. New South Wales. Geol. Survey Rec. 21, 127–226.

Butler, R.W.H., Lloyd, G.E., Holdsworth, R.E., 1997. The role of basement reactivation in continental deformation. Geol. Soc. Lond. 154, 69–71.

Campana, B., King, D., 1958. Regional geology and mineral resources of the Olary Province, South Australia. Geol. Survey Bull., 34.

Clarke, G.L., Burg, J.-P., Wilson, C.J.L., 1986. Stratigraphic and structural constraints on the proterozoic tectonic history of the Olary Block, South Australia. Precambrian Res. 34, 107–138.

Clarke, G.L., Powell, R., Vernon, R.H., 1995. Reaction relationships during retrograde metamorphism at Olary, South Australia. J. Metam. Geol. 13, 715–726.

Conor, C.H.H., (Compiler), 2004. Geology of the Olary Domain, Curnamona Province, South Australia. PIRSA Report Book, 2004/08.

Cook, N.D.F., Ashley, P.M., 1992. Meta-evaporite sequence, exhalative chemical sediments and associated rock in the Proterozoic Willyama supergroup, south Australia: implications for metallogenesis. Precambrian Res. 56, 211–226.

Corbett, G.J., Phillips, G.N., 1981. Regional retrograde metamorphism of a high grade terrain: the Willyama Complex, Broken Hill, Australia. Lithos 14, 59–73.

Davis, B.K., 1995. Regional-scale foliation reactivation and re-use during formation of a macroscopic fold in the Robertson River Metamorphics, north Queensland, Australia. Tectonophysics 242, 293–311.

Davis, B.K., Forde, A., 1994. Regional slaty cleavage formation and fold axis rotation by re-use and reactivation of pre-existing foliations: The Fiery Creek State Belt, North Queensland. Tectonophysics 230, 161–179.

De Capitani, C., Brown, T.H., 1987. The computation of chemical equilibrium in complex systems containing non-ideal solutions. Geochim. Cosmochim. Acta 51, 2639–2652.

Dutch, R.A., Hand, M., Clark, C., 2005. Cambrian reworking of the southern Australian Proterozoic Curnamona Province; constraints from regional shear zone systems. Geol. Soc. London 162 (5), 763–775.

Flint, R., 2002. Structural evolution of the Outalpa Inlier, Olary Domain, Curnamona Province. MESA J. 26, 34–41.

Flint, R.B., Parker, A.J., 1993. Willyama Inlier. In: Drexel, J.F., Preiss, W.V., Parker, A.J. (Eds). The Geology of South Australia, Vol. 1. The Precambrian. *Geol. Surv. South Aust. Bull.*, 82–93.

Forbes, C.J., Betts, P.G., 2004. Development of Type 2 fold interference patterns in the Broken Hill Block: implications for strain partitioning across a detachment during the Olarian Orogeny. Aust. J. Earth Sci. 51, 173–188.

Forbes, C.J., Betts, P.G., Lister, G.S., 2004. Synchronous development of Type 2 and Type 3 fold interference patterns: evidence for recumbent sheath folds in the Allendale Area, Broken Hill, NSW, Australia. J. Struct. Geol. 26, 113–126.

Fossen, H., Tikoff, B., 1993. The deformation matrix for simultaneous simple shearing, pure shearing and volume change, and its application to transpression/transtension tectonics. J. Struct. Geol. 15, 413–422.

Fossen, H., Tikoff, B., 1998. Extended models of transpression and transtension, and application to tectonic settings. In: Holdsworth, R.E., Strachan, R.A., Dewey, J.F. (Eds.), Continental transpressional and transtensional tectonics. Geol. Soc. London Spec. Publ., 135, 15–33.

Fry, K., Betts, P.G., 2004. Delamerian shear sense indicators in the Bulloo north area, Olary Domain, South Australia. Abstracts of Papers Presented at the February 2004 Conference in Hobart. 17th Australian Geological Convention, Record 2004/73.

Ganne, J., Bertrand, J.M., Fudral, S., Vidal, O. Structural and metamorphic evolution of the Ambin massif (Western Alps): toward a new exhumation model for the Briançonnais domain. Tectonophysics, Spec Publ., GeoFrance 3D, in press.

Gibson, G.M., 2000. Tectonic evolution of the Paleoproterozoic Willyama Supergroup: the early years, In: Peljo, M. (compiler), Broken Hill Exploration Initiative Abstracts Volume, AGSO Record 2000, 10, 45–47.

Gibson, G.M., 2002. Notes for a Broken Hill Exploration Initiative Field Workshop. In: Fabris, A.J. (Ed.) Curnamona Province information package for Olary and Mingary Field workshop. October 2002. Mineral Exploration Data Package, South Australia Department of Primary Industries and Resources.

Gibson, G.M., Nutman, A.P., 2004. Detachment faulting and bimodal magmatism in the Paleoproterozoic Willyama Supergroup, south-central Australia: keys to recognition of a multiply deformed Precambrian metamorphic core complex. Geol. Soc. Lond. 161, 55–66.

Gibson, G.M., Peljo, M., Chamberlain, T., 2004. Evidence and timing of crustal extension versus shortening in the early tectonothermal evolution of a Proterozoic continental rift sequence at Broken Hill, Australia. Tectonics 23, doi:10.1029/2003TC001552.

Giles, D., Betts, P., Lister, G.S., 2002. A far-field continental back-arc setting for the 1.80–1.67 Ga basins of northeastern Australia. Geology 30, 823–826.

Giles, D., Betts, P., Lister, G.S., 2004. 1.8–1.5-Ga links between the North and South Australian Cratons and the Early–Middle Proterozoic configuration of Australia. Tectonophysics 380, 27–41.

Glen, R.A., Laing, W.P., Parker, A.J., Rutland, R.W.R., 1977. Tectonic relationships between the Proterozoic Gawler and Willyama orogenic domains, Australia. J. Geol. Soc. Aust. 24, 125–150.

Goodge, J.W., Hansen, V.L., Peacock, S.M., Smith, B.K., Walker, N.W., 1993. Kinematic evolution of the Miller Range shear zone, central Transantarctic Mountains. Tectonics 12, 1460–1478.

Grady, A.E., Flint, D.J., Wiltshire, R.J., 1989. Excursion guide for Willyama Supergroup and related rocks, Olary district, SA. South Australia, Department of Mines and Energy. Report Book, 89/23.

Gustafson, J.K., Burrell, H.C., Garretty, M.D., 1950. Geology of the Broken Hill ore deposit, Broken Hill, NSW, Australia. Geol. Soc. Am. Bull. 61, 1369–1437.

Hand, M., Rutherford, L., Barovich, K., 2003. Garnet Sm–Nd Age Constraints on the timing of tectonism in the southwestern Curnamona Province: implication for existing models and correlations. In: Peljo, M. (compiler), Broken Hill Exploration Initiative Abstracts Volume, AGSO Record 2003, 13, 65–68.

Hanmer, S., Passchier, C., 1991. Shear-Sense Indicators: A Review. Geol. Surv. Can. Paper, 17–90, 72 pp.

Harrison, T.M., McDougall, I., 1981. Excess ^{40}Ar in metamorphic rocks from Broken Hill, New south Wales : implications for ^{40}Ar/^{39}Ar age spectra and the thermal history of the region. Earth Planet. Sci. Lett. 55, 123–149.

Hobbs, B.E, Archbald, N.J., Etheridge, M.A., Wall, V.J., 1984. Tectonic history of the Broken Hill Block, Australia. In: Kroner, A., Greiling, A. (Eds.), Precambrian Tectonics Illustrated. Schweizerbart'sche Stuttgart, pp. 353–368.

Hobbs, B.E., Means, W.D., Williams, P.F., 1976. An Outline of Structural Geology. John Wiley and Sons Inc., New York, NY, 571 pp.

Holdsworth, R.E., Butler, C.A., Roberts, A.M., 1997. The recognition of reactivation during continental deformation. J. Geol. Soc. Lond. 154, 73–78.

Hopgood, A.M., 1980. Polyphase fold analysis of gneisses and migmatites. Trans. R. Soc. Edinburgh, Earth Sci. 71, 55–68.

Jiang, D., Williams, P.F., 1998. High strain zones: a unified model. J. Struct. Geol. 20, 1105–1120.

Jiang, D., Williams, P.F., 1999. A fundamental problem with the kinematic interpretation of geological structures. J. Struct. Geol. 21, 933–937.

Jones, R.R., Holdsworth, R.E., Bailey, W., 1997. Lateral extrusion in transpression zones: the importance of boundary conditions. J. Struct. Geol. 19, 1201–1217.

Jowett, E.C., 1991. Fitting iron and magnesium into the hydrothermal chlorite geothermometer: GAC/MAC/SEG. Joint Annual Meeting, Toronto, May 27–27, 1991. Program with Abstract 16, A62.

Laajoki, K., Tuisku, P., 1990. Metamorphic and structural evolution of the Early Proterozoic Puolankajarvi Formation, Finland, 2. Structural and textural relations. J. Metamorph. Geol. 8, 357–374.

Laing, W.P., 1969. The geology of the Brewery Well area, northern Barrier Rangers, western New South Wales. Honours Thesis, University of Sydney (unpublished).

Laing, W.P., 1995. Geological Geology of the Olary Region, Scale 1:500 000. Geol. Survey of South Australia.

Laing, W.P., Marjoribank, R.W., Rutland, R.W.R., 1978. Structure of the Broken Hill mine area and its significance for the genesis of orebodies. Econ. Geol. 73, 1112–1136.

Leyh, W.R., Connor, C.H.H., 2000. Stratigraphically controlled metallogenic zonation associated with regional redox boundary of the Willyama Supergroup—economic implications for the southern Curnamona Province. MESA J. 16, 39–47.

Lin, S., Jiang, D., Williams, P.F., 1998. Transpression (or transtension) zones of triclinic symmetry: natural example and theoretical modelling. In: Holdsworth, R.E., Strachan, R.A., Dewey, J.F. (Eds.), Continental Transpressional and Transtensional Tectonics, Geol. Soc. London Spec. Publ., 135, 41–57.

Lishmund, S.R., 1982. Non-metallic and tin deposits of the Broken Hill district, NSW. Geol. Surv. Bull. 28, 1–176.

Lister, G., Snoke, A.W., 1984. S-C mylonites. J. Struct. Geol. 6, 617–638.

Marjoribanks, R.W., Rutland, R.W.R., Glen, R.A., Laing, W.P., 1980. The structure and tectonic evolution of the Broken Hill region, Australia. Precambrian Res. 13, 209–240.

Marmo, B., Clarke, G.L., Powell, R., 2002. Fractionation of bulk rock composition due to porphyroblast growth: effects on eclogite facies mineral equilibria, Pam Peninsula, New Caledonia. J. Metamorph. Geol. 20, 151–165.

Means, W.D., 1994. Rotational quantities in homogeneous flow and the development of small-scale structure. J. Struct. Geol. 16, 437–445.

Meyre, C., Zack, T., de Capitani, C., Frey, M., 1997. High-pressure metapelites of the Adula Nappe (Central Alps, Switzerland). Abstract of 5th International Eclogite Conference, Supplement No. 1 to Terra Nova 9, p. 20.

Noble, M., Betts, P.G., Forbes, C., 2004. Early structural evolution of the Curnamona province. Abstracts of Papers Presented at the February 2004 Conference in Hobart. 17th Australian Geological Convention, Record 2004/73.

Page, R.W., Stevens, B.P.J., Conor, C.H.H., Preiss, W., Crooks, A., Robertson, S., Gibson, G.M., Foudoulis, C., 2003. SHRIM U–Pb geochronology in the Curnamona Province: improving the framework for mineral exploration. In: Peljo, M. (Ed.), Broken Hill Exploration Initiative: Abstracts of Papers Presented at the July 2003 Conference in Broken Hill. Australian Geological Survey Organisation, Record 2003/13.

Page, R.W., Stevens, B.P.J., Gibson, G.M., Conor, C.H.H., 2000. Geochronology of Willyama supergroup rocks between Olary and Broken Hill, and comparison to northern Australia. In: Peljo, M. (Ed.), Broken Hill Exploration Initiative: Abstracts of Papers Presented at the May 2000 Conference in Broken Hill. Australian Geological Survey Organisation, Record 2000/10.

Parker, A.J., 1972. A petrological and structural study of portion of the Olary Province, west of Wiperaminga Hill, South Australia. University of Adelaide, B.Sc. (Hons) Thesis, unpublished.

Parra, T., Vidal, O., Agard, P., 2002. A thermodynamic model for Fe–Mg dioctahedral K–white micas using data from phase equilibrium experiments and natural pelitic assemblages. Contrib. Miner. Petr. 143, 706–732.

Passchier, C.W., 1994. Structural geology across a proposed Archaean terrane boundary in the eastern Yilgarn craton, Western Australia. Precambrian Res. 68, 43–64.

Passchier, C.W., 1998. Monoclinic model shear zones. J. Struct. Geol. 20, 1121–1137.

Powell, R., Holland, T.J.B., 1994. Optimal geothermometry and geobarometry. Am. Miner. 79, 120–133.

Preiss, W.V., 2000. The Adelalide Geosyncline of South Australia and its significance in Neoproterozoic continental reconstruction. Precambrian Res. 100, 21–63.

Raetz, M., Krabbendam, M., Donaghy, A.G., 2002. Compilation of U-Pb zircon data from the Willyama Supergroup, Broken Hill region, Australia: evidence for three tectonostratigraphic successions and four magmatic events? Aust. J. Earth Sci. 49, 985–1010.

Ramsay, J.G., 1967. Folding and Fracturing of Rocks. McGraw-Hill, New York, p. 568.

Ramsay, J.G., 1980. Shear zone geometry: a review. J. Struct. Geol. 2, 83–99.

Reddy, S.M., Collins, A.S., Mruma, A., 2003. Complex high-strain deformation in the Usagaran Orogen, Tanzania: structural setting of Palaeoproterozoic eclogites. Tectonophysics 375, 101–123.

Reddy, S.M., Occhipinti, S., 2004. High-strain zone deformation in the southern Capricorn Orogen, Western Australia: kinematics and age constraints. Precam. Res. 128, 295–314.

Rieder, M., Cavazzini, G., D'yakonov, Y.S., Frank-Kamenetskii, V.A., Gottardi, G., Guggenheim, S., Koval, P.V., Müller, G., Neiva, A.M.R., Radoslovich, E.W., Robert, J.L., Sassi, F.P., Takeda, H., Weiss, Z., Wones, D.R., 1998. Nomenclature of the micas. Clays and Clay Miner. 46, 586–595.

Robertson, R.S., Preiss, W.V., Crooks, A.F., Hill, P.W., Sheard, M.J., 1998. Review of the Proterozoic geology and mineral potential of the Curnamona Province in South Australia. J. Aust. Geol. Geophys. 17, 169–182.

Robin, P.Y.F., Cruden, A.R., 1994. Strain and vorticity patterns in ideally ductile transpression zones. J. Struct. Geol. 16, 447–466.

Rolland, Y., Cox, S.F., Boullier, A.-M., Pennachioni, G., Manktelow, N., 2003. Rare earth and trace element mobility in mid-crustal shear zones: insights from the Mont Blanc Massif (Western Alps). Earth. Planet. Sci. Lett. 214, 203–219.

Rutland, R.W.R., Etherridge, M.A., 1975. Two high grade schistosities at Broken Hill and their relation to major and minor structures. J. Geol. Soc. Aust. 22, 259–274.

Sanderson, D.J., Marchini, W.R.D., 1984. Transpression. J. Struct. Geol. 6, 449–458.

Stevens, B.P.J., 1986. Post depositional history of the Willyama supergroup in the Broken Hill Block, NSW. Aust. J. Earth Sci. 33, 73–98.

Stevens, B.P.J., Rothery, E., 1997. Delamerian refolding of the Paleoproterozoic Broken Hill Block. Aust. J. Earth Sci. 44, 275–279.

Stevens, B.P.J., Stroud, W.J., 1983. Rocks of the Broken Hill Block: their classification, nature, stratigraphic, distribution and origin. New South Wales. Geol. Survey Rec. 21, 1–323.

Stevens, B.P.J., Barnesn, R.G., Brown, R.E., Stroud, W.J., Willis, I.L., 1988. The Willyama Supergroup in the Broken Hill and Euriowie Blocks. New South Wales. Precam. Res. 40/41, 297–327.

Tikoff, B., Greene, D., 1997. Stretching lineations in transpressional shear zones: an example from the Sierra Nevada Batholith, California. J. Struct. Geol. 19, 29–39.

Tikoff, B., Teyssier, C., 1994. Strain modeling of displacement-field partitioning in transpressional orogens. J. Struct. Geol. 16, 1575–1588.

Trotet, F., Jolivet, L., Vidal, O., 2001a. Tectono-metamorphic evolution of Syros and Sifnos Islands (Cyclades, Greece). Tectonophysics 338, 179–206.

Trotet, F., Vidal, O., Jolivet, L., 2001b. Exhumation of Syros and Sifnos metamorphic rocks (Cyclades, Greece). New constraints on the *P–T* paths. Eur. J. Mineral. 13, 901–920.

Vernon, R.H., 1969. Northwestern region: Archaean or lower Proterozoic rocks, the Willyama Complex, Broken Hill area. In: Packham, G.H. (Ed.), The Geology of New South Wales. Geol. Soc. Aust., 18, 267–277.

Vernon, R.H., 1989. Porphyroblast-matrix microstructural relationships: recent approaches and problems. In: Daly, J.S., Cliff, R.A., Yardley, B.W.D. (Eds.), Evolution of Metamorphic Belts. Geol. Soc. London, Spec. Publ., 43, 83–102.

Vidal, O., Parra, T., 2000. Exhumation path of high pressure metapelites obtained from local equilibria for chlorite-phengite assemblages. Geol. J. 35, 139–161.

Vidal, O., Parra, T., Trotet, F., 2001. A thermodynamic model for Fe-Mg aluminous chlorite using data from phase equilibrium experiments and natural pelitic assemblages in the 100–600 °C, 1–25 kbar *P–T* range. Am. J. Sci. 301, 557–592.

Wheeler, J., Butler, R.W.H., 1993. An extensional contact between the oceanic Piemonte and overlying continental Sesia units, Western Italian Alps. Earth Planet. Sci. Lett. 117, 457–474.

White, S.H., Rothery, E., Lips, A.L.W., Barclay, T.J.R., 1995. Broken Hill area, Australia as a Proterozoic fold and thrust belt: implications for the Broken Hill base-metal deposit. Trans. Instit. Miner. Metal. 106, 1–17.

Willis, I.L., Brown, R.E., Stroud, W.J., Stevens, B.P.J., 1983. The Early Proterozoic Willyama Supergroup: stratigraphic subdivision and interpretation of high-to-low-grade metamorphic rocks in the Broken Hill Block, NSW. Geol. Soc. Aust. 30, 195–224.

Wilson, J.L., Powell, R., 2001. Strain localization and high-grade metamorphism at Broken Hill. Australia: a view from the Southern Cross area. Tectonophysics 335, 193–210.

Worley, B., Powell, R., Wilson, C.J.L., 1997. Crenulation cleavage formation: Evolving diffusion, deformation and equilibration mechanisms with increasing metamorphic grade. J. Struct. Geol. 19, 1121–1135.